Interferon Regulatory Factors IRF1 and IRF7 Directly Regulate Gene Expression in Bats in Response to Viral Infection

Graphical Abstract
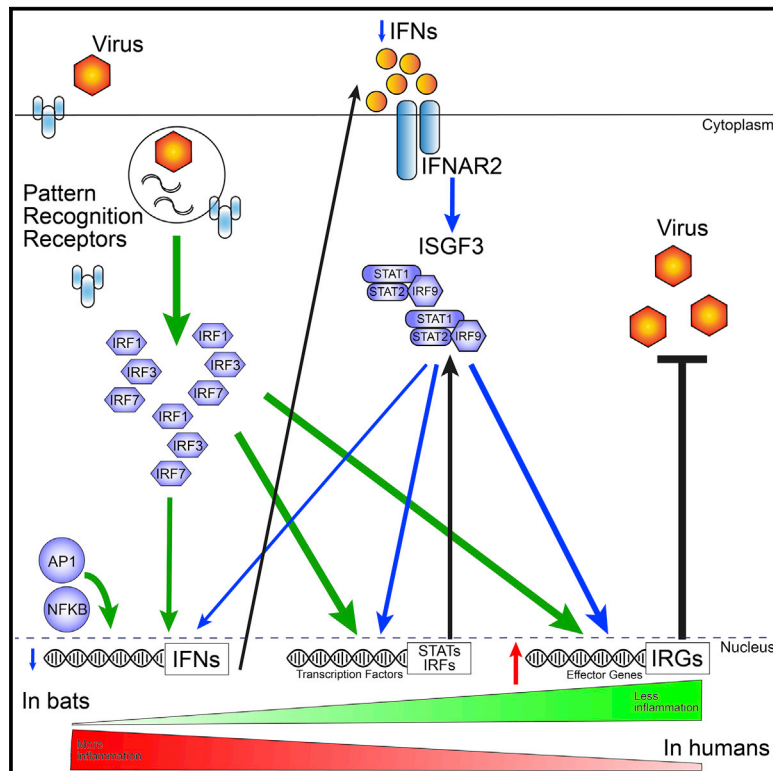
Authors

Aaron T. Irving, Qian Zhang,
Pui-San Kong, ..., Justin H.J. Ng,
Radoslaw M. Sobota, Lin-Fa Wang

Correspondence

aaronirving@intl.zju.edu.cn (A.T.I.),
linfa.wang@duke-nus.edu.sg (L.-F.W.)

In Brief

Bats express high levels of antiviral genes in response to synthetic dsRNA, IFN, or virus by the transcription factors IRF1/7. Irving et al. show that this induction largely bypasses IFNα/β production and that this may be a method for limiting the inflammation induced by IFN signaling while still restricting virus infection.

Highlights

- IRF1, 3, and 7 are highly expressed in multiple bat tissues and control gene expression

- Antiviral IRG expression in bat cells is largely IFN independent

- IRF1 and 7 regulate distinct subsets and alter the kinetics/maintenance of IRGs

- IRF1, 3, and 7 regulate antiviral responses to IAV/MERS/HSV-1/PRV3M in bat cells

CellPress

Article

Interferon Regulatory Factors IRF1 and IRF7 Directly Regulate Gene Expression in Bats in Response to Viral Infection

Aaron T. Irving,[1,2,3,8,*] Qian Zhang,[1,4,5] Pui-San Kong,[1] Katarina Luko,[1] Pritisha Rozario,[1] Ming Wen,[1] Feng Zhu,[1] Peng Zhou,[1,5] Justin H.J. Ng,[1] Radoslaw M. Sobota,[6,7] and Lin-Fa Wang[1,*]

[1]Programme in Emerging Infectious Diseases, Duke-NUS Medical School, Singapore, Singapore
[2]Zhejiang University-University of Edinburgh Institute, Zhejiang University School of Medicine, Zhejiang University International Campus, Haining, China
[3]Second Affiliated Hospital, Zhejiang University School of Medicine, Hangzhou, China
[4]University of Chinese Academy of Sciences, Beijing, China
[5]Key Laboratory of Special Pathogens, Wuhan Institute of Virology, Chinese Academy of Sciences, Wuhan, China
[6]Functional Proteomics Laboratory, Institute of Molecular and Cell Biology (A*STAR), Singapore, Singapore
[7]Institute of Medical Biology (IMB), Agency for Science, Technology and Research (A*STAR), Singapore, Singapore
[8]Lead Contact
*Correspondence: aaronirving@intl.zju.edu.cn (A.T.I.), linfa.wang@duke-nus.edu.sg (L.-F.W.)
https://doi.org/10.1016/j.celrep.2020.108345

SUMMARY

Bat cells and tissue have elevated basal expression levels of antiviral genes commonly associated with interferon alpha (IFNα) signaling. Here, we show Interferon Regulatory Factor 1 (IRF1), 3, and 7 levels are elevated in most bat tissues and that, basally, IRFs contribute to the expression of type I IFN ligands and high expression of interferon regulated genes (IRGs). CRISPR knockout (KO) of IRF 1/3/7 in cells reveals distinct subsets of genes affected by each IRF in an IFN-ligand signaling-dependent and largely independent manner. As the master regulators of innate immunity, the IRFs control the kinetics and maintenance of the IRG response and play essential roles in response to influenza A virus (IAV), herpes simplex virus 1 (HSV-1), Melaka virus/Pteropine orthoreovirus 3 Melaka (PRV3M), and Middle East respiratory syndrome-related coronavirus (MERS-CoV) infection. With its differential expression in bats compared to that in humans, this highlights a critical role for basal IRF expression in viral responses and potentially immune cell development in bats with relevance for IRF function in human biology.

INTRODUCTION

Bats are unique mammals with physiological capabilities including elevated metabolism (McNab, 1989; O'Mara et al., 2017; Shen et al., 2010; Suarez and Welch, 2017; Thomas, 1975) and flight (Suarez et al., 2009a, 2009b; Thomas, 1975; Zhang et al., 2013). Some bats are capable of torpor/hibernation without drastic energy requirements (Bouma et al., 2010; Currie et al., 2018; Han et al., 2015). Bats from most species are long-lived with some having exceptional longevity quotients relative to their body size (Austad and Fischer, 1991; Brunet-Rossinni, 2004; Brunet Rossinni, 2004; Foley et al., 2018; Huang et al., 2016; Podlutsky et al., 2005). They share common features including minimal systemic inflammation, fever, or clinical disease upon viral infection (Cabrera-Romo et al., 2014; Davis et al., 2005; Paweska et al., 2016; Perea-Martínez et al., 2013; Reagan and Brueckner, 1952; Simpson and O'Sullivan, 1968; Stockmaier et al., 2015). Several groups have highlighted a heightened innate immune system, baseline interferon (IFN) signatures, and basal IFN-ligand expression (Baker et al., 2013;

Fuchs et al., 2017; Pavlovich et al., 2018; Zhang et al., 2013, 2017; Zhou et al., 2016). Nonetheless, the adaptive immune responses, particularly antibody development and production, are somewhat limited (Davis et al., 2005; Herbold et al., 1983; Jones et al., 2019, 2015; Middleton et al., 2007; Obregón-Morales et al., 2017; Paweska et al., 2016; Suu-Ire et al., 2017; Swanepoel et al., 2007; Yong et al., 2018). Despite infection and shedding, bats do not succumb to most viral infections, even when experimentally infected with highly pathogenic zoonotic viruses. Studies have shown transient inflammation or mild disease that is soon resolved by the bat immune system (Jones et al., 2019).

Previously, we showed fruit bat cells deficient in part of the type-I IFN receptor IFNAR2 maintain the imprinted "antiviral signature" (Zhang et al., 2017), indicating the baseline interferon regulated gene (IRG) expression did not result from basal canonical IFN signaling. Although Interferon Regulatory Factors (IRFs) in humans control additional genes to type I IFN-ligands, their contribution to immunity is predominantly believed to be by IFN-ligand induction, rather than directly on IRGs (Andrilenas
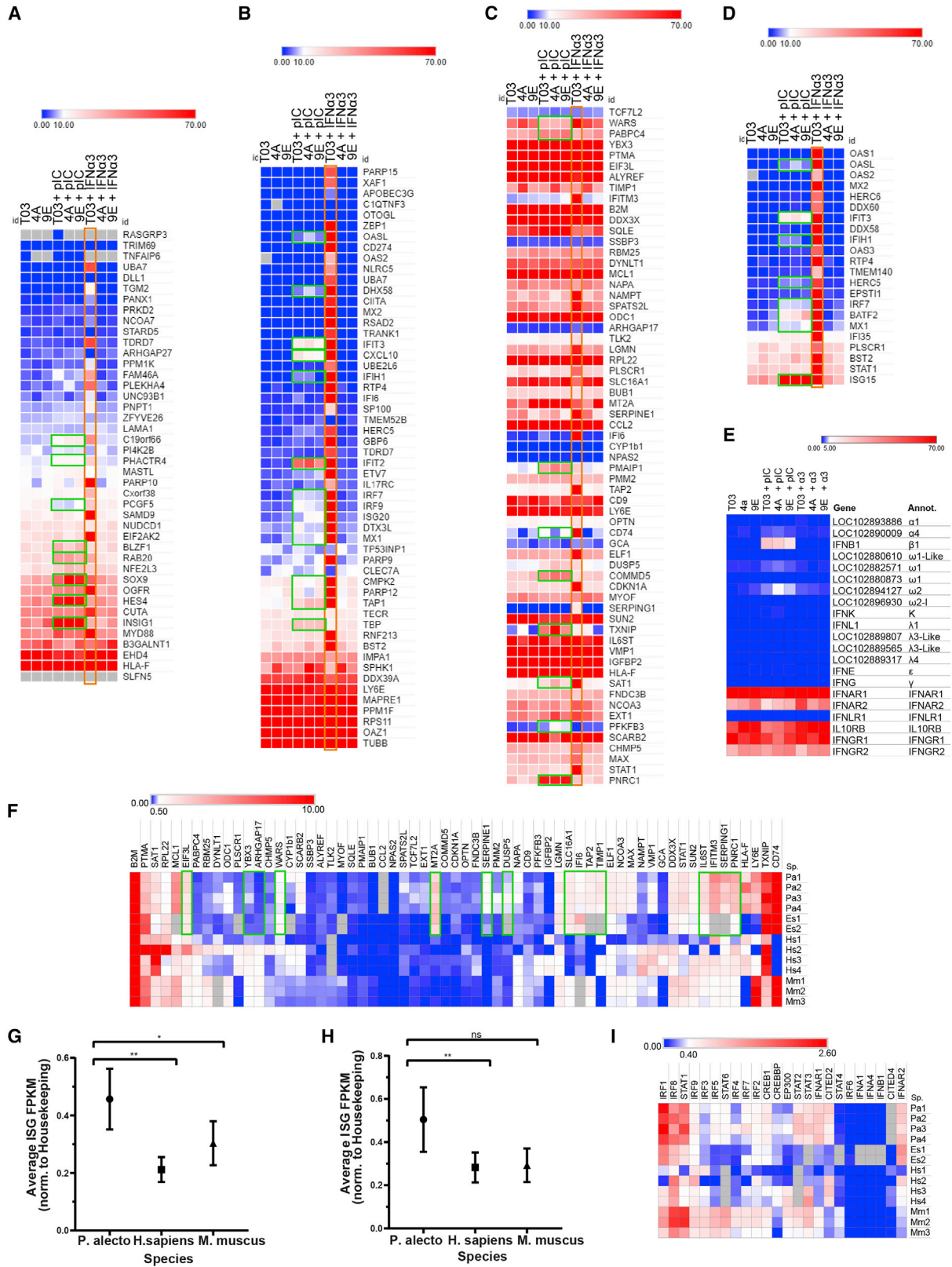
(legend on next page)

et al., 2018; Ashley et al., 2019; Barnes et al., 2004; Cohen et al., 2014; Dery et al., 2018; Honda et al., 2005; Langlais et al., 2016; Eggenberger et al., 2019; Piya and Kim, 2018; Schmid et al., 2010; Shultz et al., 2009; Wang et al., 2017; Yu et al., 2018). IRF3 is more well-studied in this regard, although studies also suggest IRF1 and 7 contribute by inducing IFNs (Andrilenas et al., 2018; Kawai et al., 2004; Li et al., 2014a; Weiss et al., 2012; Zhou et al., 2012, 2015). IRF7 from the Australian black flying fox *Pteropus alecto*, has been highlighted as a potent regulator of interferon alpha (IFNα). Unlike the restriction to lymphoid cells/monocytes seen in most mammals, IRF7 is expressed in several tissues (Zhou et al., 2014). Bat IRF7 has a conserved DNA-binding domain, similar to that in humans, with an expanded myd88-binding region that from preliminary studies appears to function as per normal. Compared with that in humans, IRF7 in bats is considerably more potent in driving the IFN promoter. However, discrepancies over IFN expression across different bat species remain, with most species exhibiting limited IFN induction. Thus, understanding bat-specific IRF functions and regulation of this high-baseline antiviral activity in bats may be critical for controlling viral infection in humans. Here, we characterize IRF1/3/7 expression levels across tissues and the role of IRFs in gene induction, basally or post-induction. Additionally, we highlight the importance of IRFs in inducing IFN-independent antiviral responses in bat cells infected with herpes simplex virus 1 (HSV-1), Middle East respiratory syndrome-related coronavirus (MERS-CoV), influenza A virus (IAV), and Melaka virus/Pteropine orthoreovirus 3 Melaka (PRV3M).

RESULTS

High-Baseline IRG Signatures Are Not Induced by IFN Ligands

IFNAR2 CRISPR knockout (KO) was used to deplete the type-I IFN receptor in *P. alecto* PakiT03 cells (clones 4A, 9E). Although these clones no longer respond to the IFNα3 ligand, they still maintain a basal signature associated with IFN (Zhang et al., 2017). We treated these clones with the double-stranded RNA (dsRNA) mimic polyIC for 3 h to observe the induction of IRGs by next-generation sequencing (NGS) transcriptomics, independent of canonical type I IFN signaling (Table S1). A classic Interferon Stimulated Gene Factor 3 (ISGF3)-STAT1/STAT2/IRF9 transcription factor (TF) signature (Figure 1A), a common/pan anti-viral IRG signature (Figure 1B) (La Cruz-Rivera et al., 2017;

Schoggins and Rice, 2011), and a recently published embryonic hematopoietic stem cell (eHSC) IRG signature (Figure 1C; Wu et al., 2018), or a u-ISGF3 unphosphorylated STAT1/2 signature (Figure 1D; Cheon et al., 2013; Sung et al., 2015; Zhou et al., 2016) were partially seen. These data show that IRG subsets are rapidly upregulated by polyIC, a synthetic dsRNA that mimics viral RNA, in the absence of type-I IFN signaling, at early time points. This response was not due to induction of IFNγ/λ as the IFNγ ligand was not expressed and neither was the IFNλ receptor IFNLR1 (Figure 1E). Similarly, the IRG signature associated with polyIC in IFNAR2-KO cells did not match that of IFNG from gene set enrichment analysis (GSEA) (Figure S1A), although IFNα treatment in wild-type (WT) cells did to some degree. Minimal IFNα ligand was detected basally and IFNβ was not. Some minor induction was observed with both IFNα3/polyIC treatment, although it was minimal, particularly compared to previous studies in humans/mice. It is, therefore, likely the direct upregulation of IRGs is induced by regulators independent of IFN ligands. The basal expression of components of the IFN signaling cascade in clonal cell lines is largely consistent. This is, therefore, unlikely the result of u-ISGF3 signaling from a high expression of STAT1/STAT2 and/or IRF9 without induction. Notably, rapid upregulation of IRF1/7 was seen in response to IFNα and IRF1 to polyIC, respectively (Figure S1B).

To ensure the baseline IRG status is consistent *in vivo*, we examined the transcriptome from healthy adult *P. alecto* and *Eonycteris spelaea* spleen (wild-born) and compared them to publicly available data from middle-aged healthy humans and adult mice (prepared with the same pipeline). To minimize inter-species variation, the data were normalized to the geometric mean of 13 housekeeping genes. The hESC IRG geneset signature is shown in Figure 1F. Although the expression varies among species, the trend is consistent with that of *P. alecto* with higher baseline IRG expression. Some notably higher genes include WARS, SERPINE1, MT2A (LOC102886224), SLC16A1, IFI6, TAP2, TMP1, IFITM3, SERPING1, and PNRC1. Although the anti-viral IRG geneset had a similar trend, the average expression in an unstimulated state (Figure S1C) was insignificant for the whole signature (*en-bulk*), *in vivo*. *E. spelaea* was removed from the subsequent genesets due to poor annotation of the genome. Significantly differential expression profiles were seen for the ISGF3 (Figures 1G and S1D) and u-ISGF3 signatures (Figures 1H and S1E). Additional IRGs differentially regulated, basally, between *P. alecto* and human spleen are also observed

---

Figure 1. IFN-Independent Regulation of Interferon Regulated Genes

(A) Heatmap of ISGF3-regulated IRG in wild-type (WT) Paki cells (T03) or IFNAR2-KO clones (4A/9E) at basal state or treated with transfected polyIC (pIC) (1 mg/ml) or *P. alecto* IFNα3 (1,000 U/ml) for 3 h as measured by NGS. Orange box highlights the IFN-treated IRG response (expected), and green boxes highlight IRG-regulated controls still up/downregulated in the absence of IFNAR2 by polyIC. Scale is for average FPKM from blue-white-red for 0-10-70 (as indicated). Most genes are thought to be only responsive to ISGF3 and not to other elements like GAS or nuclear factor κB (NF-κB).

(B) As per (A) for the unphosphorylated-ISGF3 (u-ISGF3) subset of IRGs.

(C) As per (A) for the antiviral IRG-subset.

(D) As per (A) for the human embryonic stem cells (hESCs) IRG subset.

(E) As per (A) for all annotated IFN transcripts in the *P. alecto* genome, with both gene symbol and annotated gene name displayed.

(F) Heatmap of IRG gene expression from spleen of *P. alecto* (n = 4), *E. spelae* (n = 2), *Homo sapiens* (n = 4), or *Mus muscus* (n = 3) shown as relative FPKM (FPKM/geometric mean of 13 housekeeping gene FPKMs) for hESC IRG subset as per (D); scale as indicated (based on min/med/max).

(G) Cumulative graph of IRG relative FPKMs as per (F) for the ISGF3-IRG subset without *E. spelaea* due to multiple unannotated genes. Error bars are SEM.

(H) As per (F) for the uISGF3-IRG -subset. Significance determined with unpaired t test; **p < 0.02, *p < 0.05.

(I) Heatmap of relative FPKM (as per F) for components of the IFN signaling pathway.
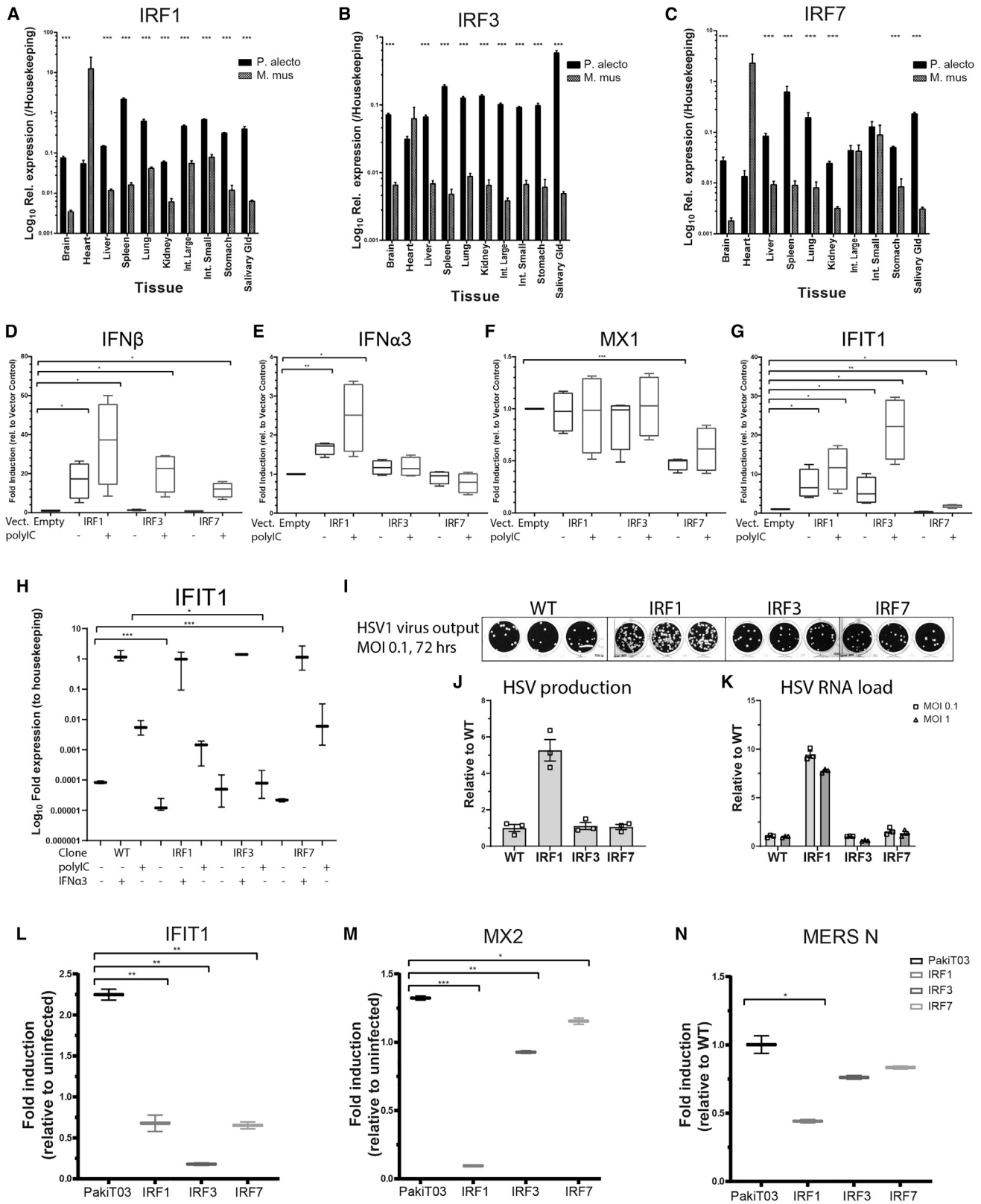
(legend on next page)

(Figure S1F). Although there are minor differences in IFN signaling machinery, including STAT1 (speculated to affect baseline IRG expression) (Figure 1I), both IRF1 and IRF7 levels remain high. These IRFs are implicated largely in the IFN responses of immune cells only, whereby IRF3 is predominant in most cell types. IRF7 is considered more important in amplification of an antiviral response, post-induction (Sharma et al., 2003).

IRFs Are Highly Expressed across Bat Tissues *In Vivo*

To validate expression, IRF1 mRNA levels were examined using a cDNA panel generated from 10 tissues isolated from 3 bats/mice (Figure 2A). *P. alecto* tissue had 1 to 2 log higher expression in the brain, liver, spleen, lung, kidney, intestine, stomach, and salivary glands than mice. IRF1 activation is poorly understood, although high expression leads to spontaneous activation in the absence of stimuli (Garvin et al., 2019; Lin and Hiscott, 1999; Shultz et al., 2009). Similarly, IRF3 expression was more prominent in bats, except for the heart tissue (Figure 2B). Likewise, IRF7 expression was higher in most bat tissues (Figure 2C) including brain, liver, spleen, lung, kidney, stomach, and salivary gland. Compared with humans, NGS transcriptomic expression from bat tissues was higher in spleen, lung, and liver in both *P. alecto* and *E. spelaea* (normalized as per Figure 1I; Figure S2A). Although IRF7 is believed to be activated in a similar fashion to IRF3, by TBK1, IKKε, or IRAK1 and IKKα, its expression is largely limited to lymphoid cells and dendritic cell subsets in humans (reviewed in Génin et al., 2009). Although IRF3/7 have additional autoinhibitory motifs, alleviated in response to dsRNA by TBK1 serine phosphorylation, IRF3 has limited function without stimulation. IRF7 is known to have an additional element increasing both basal and virus-induced activity (Lin et al., 2000a) and is considered more promiscuous with its binding motif (Lin et al., 2000b). To this end, we observed spontaneous nuclear localization of IRF1 and partially for IRF7-GFP fusion constructs, which were use used previously (Zhou et al., 2014), in PakiT03 cells after 12 h from expression alone. IRF3-GFP required 90 min of stimulation with polyIC for optimal nuclear localization (Figure S2B). IRF7-GFP can be seen in sub-nucleolar structures (speckles) both before and enhanced after polyIC stimulation. Compared to that of humans, bat IRF7 appears to have greater nuclear localization in the absence of stimulation (Lin et al., 2000a, 2000b). This matches the observation of IFNβ induction in response to IRF3 and 7 requiring polyIC induction (Figure 2D). We tested if IRF1 drove bat IFNα promoters, similar to IRF7 (Zhou et al., 2014). IRF1 was the strongest driver of all three characterized IFNα promoters in *P. alecto*, followed by IRF7 and IRF3 (Figure S2C); notably, this was in the absence of polyIC for which induction is solely by basal expression. Thus, the major limiting factor for IRF1/7 activity may be its lack of expression, although IRF7 can be enhanced by dsRNA.

IRF1 and IRF7 Regulate Antiviral Genes Basally

To examine IRF regulation on key IRGs during antiviral responses, we examined IFNα3 (Figure 2E), IFNβ (Figure 2D), MX1 (Figure 2F), and IFIT1 (Figure 2G) mRNA expression by using IRF1/3/7-GFP fusion constructs. To eliminate IFN-induced gene induction, IFNAR2 KO cells were treated with and without intracellular polyIC stimulation for 3 h (1 μg/ml). IFNα3 expression was induced with and without polyIC by IRF1 although not by IRF3/7. IFNβ was induced by IRF1/7, with or without polyIC treatment, although it enhanced for IRF7 with polyIC. Inversely, IRF7 overexpression suppressed MX1 and IFIT1; however, this was partially alleviated by polyIC induction. IRF1 basally induced IFIT1 unexpectedly, whereas IRF3-expressing cells required polyIC induction to achieve full expression of IFIT1, fitting with the luciferase and nuclear localization observations. A mild IRF-suppressive effect was observed for BST2 and STAT1 but not for Rig-I (Figures S2D–S2F). This suppressive IRF effect on MDA5 and PKR was alleviated by polyIC stimulation (Figures S2G and 2H). To confirm IRF overexpression was not working by compensatory induction of IFNγ/λ, we treated the same cells with the Jak inhibitor ruxolitinib. Control and IFN-α3-stimulated cells showed a similar absence of IRG-induction profiles, as measured by a previously described nanostring panel (Irving et al., 2020), whereas ruxolitinib-treated cells with IFNα3 showed a slight increase, possibly indicating a degree of interference from IFNAR1 binding in the absence of IFNAR2. Fitting with the idea of Jak-STAT-signaling-independent, direct/indirect IRF-dependent induction, ruxolitinib actually enhanced IRF-overexpression-induced IRG induction, particularly with genes such

---

Figure 2. The Role of IRFs in Intrinsic Innate Immunity

(A) qPCR of IRF1 ($\log_{10}$ of relative expression/geometric mean of housekeeping across all tissues) for various bat (*P. alecto*) and mouse (*M. muscus*) adult tissue cDNA panels (n = 3 each).

(B) As per (A) for IRF3.

(C) As per (A) for IRF7. Significance is as indicated (multi-row unpaired t test by tissue); ***p < 0.01.

(D) qPCR of fold induction of IFNβ gene (relative to vector only control) for PAkiT03-4A IFNAR2 KO CRISPR cells transfected with control vector, IRF1, IRF3, or IRF7 with or without polyIC treatment (normalized to housekeeping, n = 4).

(E) As per (D) for IFNα3 gene induction.

(F) As per (D) for MX1 gene induction.

(G) As per (D) for IFIT1 gene induction. Significance determined with unpaired t test with Welch's correction; ***p < 0.01, **p < 0.02, *p < 0.05.

(H) qPCR of IFIT1 expression ($\log_{10}$, relative to housekeeping expression) in PakiT03 (WT) cells or IRF1/3/7 CRISPR KO clones treated with polyIC or IFNα3 for 3 h, as previously stated.

(I) Titration on Vero cells with 2% methyl-cellulose of HSV-1 in the supernatant of WT or IRF1/3/7/ KO clones after infection with HSV at an MOI of 0.1 for 72 h.

(J) Quantification of the titration in (I), as plaque-forming unit (PFU)/ml.

(K) qPCR of HSV-1 ICP0 (relative to the geometric mean of WT) from RNA of infected cells as per (I) at an MOI of 0.1 or 1 for WT or IRF1/3/7 KO cells.

(L) qPCR of IFIT1 (fold induction compared to uninfected) in PakiT03 WT or IRF1/3/7 KO cells following infection with MERS-CoV at an MOI of 0.1 for 48 h.

(M) As per (L) for MX-2 gene induction.

(N) As per (L) for MERS-CoV N gene induction (relative to WT infected). Significance determined with unpaired t test; ***p < 0.01, **p < 0.02, *p < 0.05 (n ≥ 3). All error bars are indicated as SEM.

as XAF1, ZBP1, TLR6, RTP4, OASL, NLRC5, MX2, IFIT2/3, CXCL10, CIITA, and APOBEC3G (Figure S2I).

To examine the impact of IRF1/3/7 in antiviral responses, we generated IRF CRISPR KO cells. Multiple CRISPR clonal cell lines were sequenced (Key Resources Table) and screened for the expression of IRGs, including BST2, IFNα3, and STAT1 (Figures S2J–S2L). IRG induction was consistently affected for multiple clones of each IRF KO, indicating a consistent trend regardless of the individual clone line. Although both qPCR and NGS data validated decreased and partial transcripts, we were unable to verify the protein level due to the lack of specific antibodies to bat IRFs. We selected clones IRF1-g4-1D, IRF3-g4-2H, and IRF7-3C for the remainder of the study and referred to them as IRF1/3/7 CRISPR KO cells.

IRF1/3/7 Alter the Response to Ligand or Infection with HSV-1, IAV, and MERS-CoV

To interrogate this response with immuno-stimulation, we treated WT or IRF1/3/7 CRISPR KO cells with polyIC or IFNα3 (as previously mentioned). Basal expression of IFIT1, measured by qPCR, is maintained by high-baseline IRF1 and 7 levels (Figure 2H) IRF3 induction requires polyIC, whereas IFNα3 can induce IFIT1 in the absence of either IRF. In response to HSV-1 infection (multiplicity of infection [MOI], 0.1; 72 h), PakiT03 cells require IRF1, but not IRF3 or 7, to restrict HSV-1 viral load, as detected by titration of the supernatant (Figures 2I and 2J) and ICP0 mRNA expression (Figure 2K). In response to IAV infection (MOI, 0.1; 72 h; H1N1 A/NWS/33), IRF3 increases the production of infectious IAV particles; however, all three IRFs are required to minimize the IAV RNA amount (Figure S2M). Similar to IRF3 regulation (Banerjee et al., 2019), all three IRFs were required for full induction of IRGs, such as IFIT1 and MX2 (Figures 2L and 2M), during MERS-CoV infection (MOI, 0.1; 48 h). Partial induction of MX2 occurred in the IRF7 KO cells, suggesting an effect on a specific subset of IRGs. MERS-CoV N gene expression was reduced in the absence of all three IRFs (Figure 2N). However, this was confounded by abundant cell death indicated by GAPDH reduction (Figure S2N). Further studies on infection kinetics, regulation of pro- and antiviral genes, and subsequent viral loads would, therefore, be required for a complete analysis of each IRF within the context of infection.

IRF-Mediated Regulation of Gene Expression in the Basal State

IRF-regulated genes were detected in the basal/unstimulated state by NGS in each CRISPR KO cell line. Genes that were significantly changed (>2-fold, p < 0.05) for IRF1, 3, and 7 are shown in Figures 3A–3C. Differentially Expressed Gene (DEG) analysis by HTseq-count/EdgeR were performed by comparing transcript expression to the WT control. These findings demonstrate the specific and overlapping up- (Figure 3D) and downregulated (Figure 3E) genes (summarized in Table S2). Compared with basal WT expression, most IRGs in the antiviral IRG geneset (Figure 3F) are affected by baseline IRF expression in bat cells, with the greatest effect in IRF1 and IRF7. This finding is consistent with earlier qPCR analysis (Figures 2H and S2J–S2L), which suggests this to be a common trend to the respective IRF KO;

however, further validation in additional cell lines and different bat species would be ideal. Consequently, the hESC IRG-geneset (Figure S3A) and ISGF3 (Figure S3B) and u-ISGF3 genesets (Figure S3C) are all affected in a gene- and IRF-specific manner. Basally, there were limited changes to type I IFN ligand expression (<2-fold). Mild decreases in IFNω2/ε/α1 were observed in IRF1-deficient cells and with all IFNs except IFNκ/ε/α3 (annotated as α4 in the current genome assembly) from IRF7 deficiency (Figure S3D). This result suggests that IRF1/7 drive IFN ligands basally, although complete removal of IRF1 or 7 suppresses IFNα4 and IFNα4/κ/ε expression, respectively. This suggests differential promoter regulation between the type I IFNs that may warrant further investigation. The majority of DEGs detected from basal regulation are unique compared to human biology, with only minimal overlap between known IRF1-transcriptional targets from the Encode database, chromatin immunoprecipitation (ChIP) assays performed in monocytes, or compared to other TFs in the CHEA 2016 database by EnrichR analysis (Figure S3E; Kuleshov et al., 2016). Likewise, there is minimal overlap between IRF3-KO DEGs and previously published IRF3-transcriptional targets in humans (Figure S3F), although limited information on IFN-independent, IRF3-dependent induction is available. IRF7 has no ChIP sequencing (ChIP-seq) data in the public databases, and yet, the DEGs from IRF7-KO cells show minimal overlap to a transcriptional profile seen from constitutively active IRF7 or SUZ12, a TF repressor identified by EnrichR with partial overlap to the IRF7 DEGs (Figure S3G). The unique gene profiles only partially correlate with other known TFs. The complete DEG heatmap with each IRF KO is shown in Figure S3H, indicating clusters of genes up-or downregulated.

Next, we analyzed the functional impact from each IRF by ingenuity pathway analysis (IPA) (Figure 3G). Very few pathways were directly associated with "antiviral responses"; rather, pathways identified involved basic metabolism, glycolysis, intracellular lipids, tryptophan metabolism, and reactive oxygen species/nitric oxide (ROS/NO) signaling. Although many pathways were significantly enriched by the DEGs (p value), the Z scores indicated that very few had an overall up-or downregulation. Collectively, this result suggests the pathways are dysregulated (i.e., some genes upregulated, some genes downregulated). Overall, the data indicate that although basal IRF expression contributes significantly to the antiviral state, a large number of DEGs invoke differential pathways to those previously observed in humans/mice. These pathways may no longer follow normal rules for regulation due to interference by high basal IRF expression.

Activation of IFN/Antiviral Pathways and Non-antiviral Pathways by polyIC

One of IRFs' key functions is their immediate response to Pattern Recognition Receptors (PRRs) from pathogens. To examine this further, we stimulated the CRISPR KO cells with transfected polyIC (pIC) and IFNα ligand. DEGs were selected as being differentially expressed (>1.5-fold change to WT, p < 0.05) if present at two time points post-treatment. IRF1/3/7, IFNAR2, or IFNAR2/IRF7 double CRISPR KO cells were examined at 6 h or 9 h post-polyIC stimulation (Figure 4A). The DEG heatmap (>2-fold
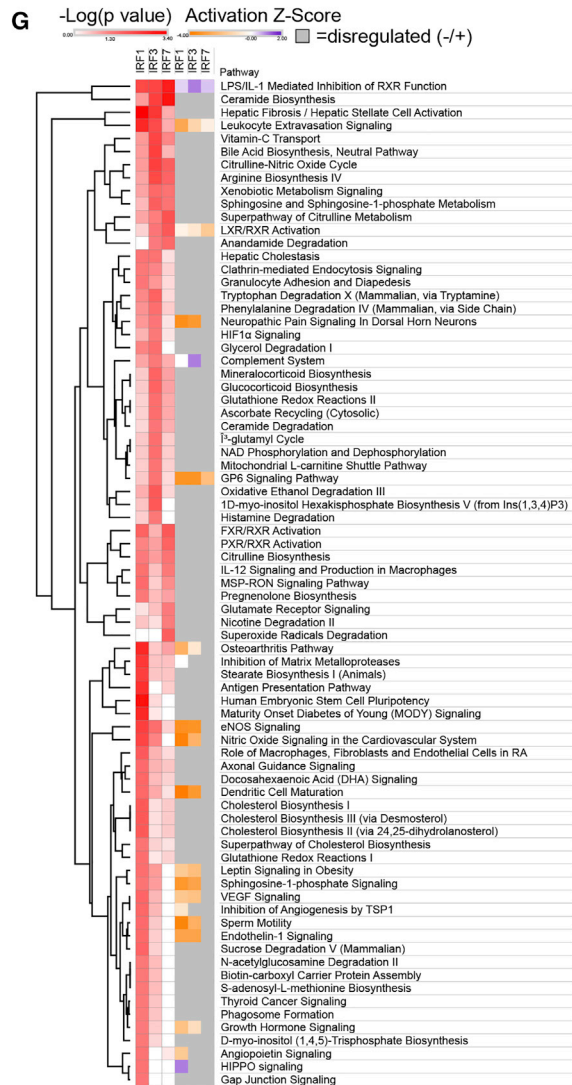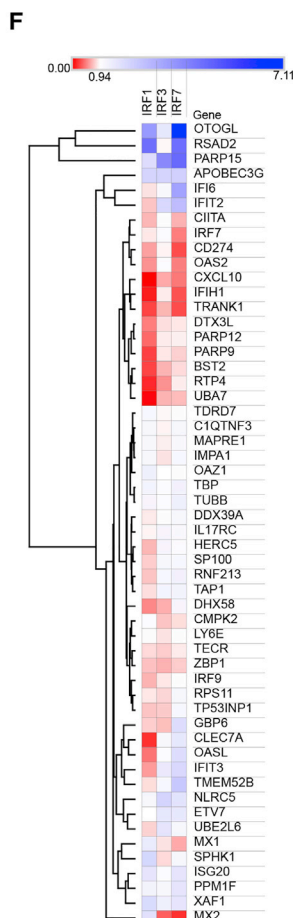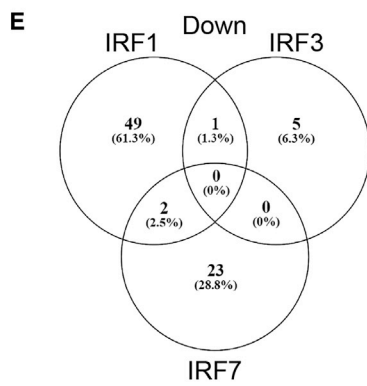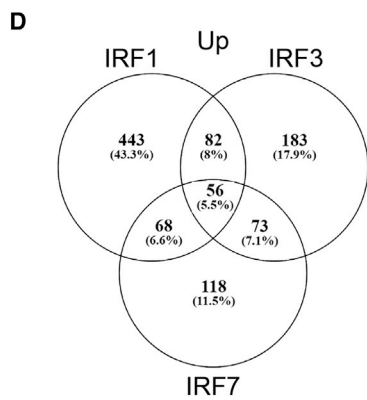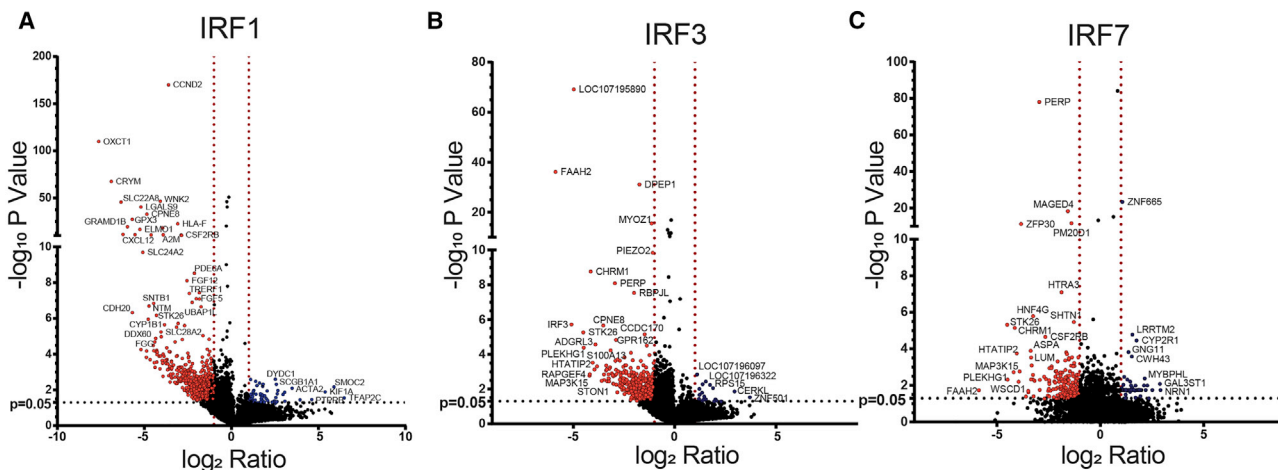
(legend on next page)

change, graphed by row *Z* score) displays distinct clusters of genes associated with each regulator or in combination with IF-NAR2 deficiency (Figures S4A and S4B). Overall, IRF1 had the largest transcriptional regulation capacity. However, there were specific IRF7-regulated genes in the presence/absence of intact IFN-signaling, highlighting IFN-dependent and -independent gene expression by IRF7. Similar pathways to basal expression (Figure 3G) were revealed by IPA at 6 h by using p value (significance; Figure 4B) or expression weighting (*Z* score; Figure 4C; Table S4). Additional pathways are also seen, including ILK/interleukin-8 (IL-8)/IL-12 signaling, dendritic cell (DC) maturation, immune cell migratory pathways, and IFN-independent IRF1/7 downregulation of NO/ROS production. Intact IFNAR2 upregulates IL-8, ILK, and CXCR4 signaling pathways, even with minimal IFN-ligand induction by polyIC (Figure S4C). GSEA scores for the signature "response to IFNα" showed a dependency of IRF3/IFNAR2 in response to polyIC (Figure 4D). Although the "IFN antiviral signature" showed a dependency only for IRF3 (Figure 4E), the "Interferon Regulated Genes induced from RSV ΔNS1 infection" displayed a dependency for IRF1/3 and IFNAR2 for significant enrichment of this geneset (Figure 4F). Intriguingly a similar enrichment score was observed for "IFN antiviral signature" by 9 h post-polyIC, even in IFNAR2 KO cells, indicating a rapid IRG induction in the absence of IFN signaling. This finding indicates specific IRF regulation of a subset of relevant IRGs. Potential upstream transcriptional regulators, such as UCP1, HNF1A/4A, TRIM24, LHX1, TICAM1, and ESR2, are highlighted compared to WT cells and may be involved in this signaling cascade (Figure S4D).

Comparing IRF-regulated genes at the 6 h or 9 h time point for BST2, MX1, and RNASEL alludes to IRF1/7 controlling the kinetics of IRG activation (Figures S4E–S4G). This is emphasized by the antiviral IRG geneset as a heatmap of fold induction, relative to untreated cells, for each time point (Figure S4H). The absence of IRF1, 3, and 7, decreased the antiviral signature at 6 h; however, IRF1 deficiency specifically enhanced IFIT2, RSAD2, CXCL10, DHX58, and OASL expression at both time points. IRF3 deficiency abrogated the signature at 9 h; yet, only some genes were IRF7 induced, suggesting subtle differences between IRF3/7. A validation of these kinetics was done by qPCR for IFIT1 at 0 h, 1 h, 3 h, 6 h, 9 h, and 24 h post-polyIC stimulation (Figure 4G). IRF1 plays a significant role in baseline IFIT1 expression; yet, any role in induction is lost by 9 h.

Conversely the role of IRF3 is most significant at 6 h post-stimulation, suggesting it requires more time for polyIC-induced expression. However, IRF7 was necessary to sustain long-term (24 h) IFIT1 induction.

IRF-Mediated Responses to IFN Are Time Dependent
To examine if IRF1/3/7 are involved in positive feedback post-IFNα-stimulation, the cells were analyzed by NGS at 3 h, 6 h, and 9 h. Compared with the WT, the IRF1/3/7 KO cells showed a unique set of genes differentially expressed (Figure 4H; p < 0.05, >2-fold induction, DEG analysis in 2 of 3 time points by EdgeR) throughout time (Figure S4I), with 486 DEGs significant across all three time points (Table S3). IPA revealed genes associated with IFN, death receptor, and IRF activation pathways (Figure 4I). There are several metabolic, intracellular lipid signaling, and ROS/NO production pathways that are downregulated post-stimulation, with downregulation exacerbated in IRF7 KO cells. Compared to the WT, additional pathways are affected independently by IRF1, 3, or 7. However, IRF7 is most notable where it maintains the IFN response at later time points, largely independent of the expression of IFNs (by positive feedback loop), as the absence of IRF1/3/7 had a minimal effect on IFN levels. Thus, these findings indicate redundancy among the IRF molecules for IFN induction, in contrast to human and mouse epithelia (Figure S4J). There was an absence of induction in WT cells by 3 h, with even partial transcriptional suppression of IFNα4/ω2 observed. This culminates in minimal upregulation by 9 h post-stimulation compared to human or mouse systems, indicating an active block of IFN ligand transcription. This has been observed in other bat species/cells previously (Glennon et al., 2015; Hölzer et al., 2019). Removal of IRF1/3 or 7 increased the positive feedback effect on IFN. Basal type-I IFN expression and an active transcriptional suppressor of IFN induction have been speculated previously in bat cells (Zhou et al., 2016). This suppressor may, therefore, be an IRF target gene, in response to IFNα. Despite only minor differences in IFN ligand expression, the absence of IRF7 at late time points led to partial dampening of the antiviral IRG geneset. IRF7 was most important for the early induction of IFI6, ISG20, BST2, DHX58, and OASL. IRF1 expression is critical for a subset of IRGs, including MX2, CD274, ISG20, GBP6, UBE2L6, C1QTNF3, CLEC7A, TRANK1, and PARP15 (Figure S4K).

Figure 3. IRF-Regulated IRGs without Induction
(A) Volcano plot for genes differentially expressed (>2-fold change, p < 0.05) calculated by EdgeR in IRF1 CRISPR KO cells at the basal state compared to parental WT PakiT03 cells. Expressed as average −log$_{10}$ p value versus log$_2$ ratio. Intersecting lines indicate p = 0.05 and 2-fold change. Genes with a decreased expression in IRF1 KO cells (red) have expression driven by IRF1, and increased expression in KO (blue) indicates downregulation by IRF1. Data as per Table S2; n = 3 replicates each.
(B) As per (A) for IRF3 CRISPR KO cells.
(C) As per (A) for IRF7 CRISPR KO cells.
(D) Venn diagram indicating IRF-specific and shared basally upregulated genes by IRF1/3/7 without induction (i.e., downregulated in KO cells), following the same cutoffs.
(E) As per (D) for downregulated genes.
(F) Example IRG geneset (antiviral IRGs, as previously mentioned) for IRGs regulated by IRF1/3/7 without induction. Scale as indicated (min/med/max) for average fold induction compared to WT, clustered based on Euclidian distance.
(G) Ingenuity pathway analysis (IPA) of the genes in Figure S3A showing the significantly changed pathways with either IRF1, 3, or 7 CRISPR KO cells. Graph scale shows significance of the pathway (−log(p value)) and activation *Z* score, whereby a negative *Z* score in the KO indicates that IRF upregulates the pathway. Grey boxes indicate significantly divergent pathways with a mix of up/downregulation of the genes.
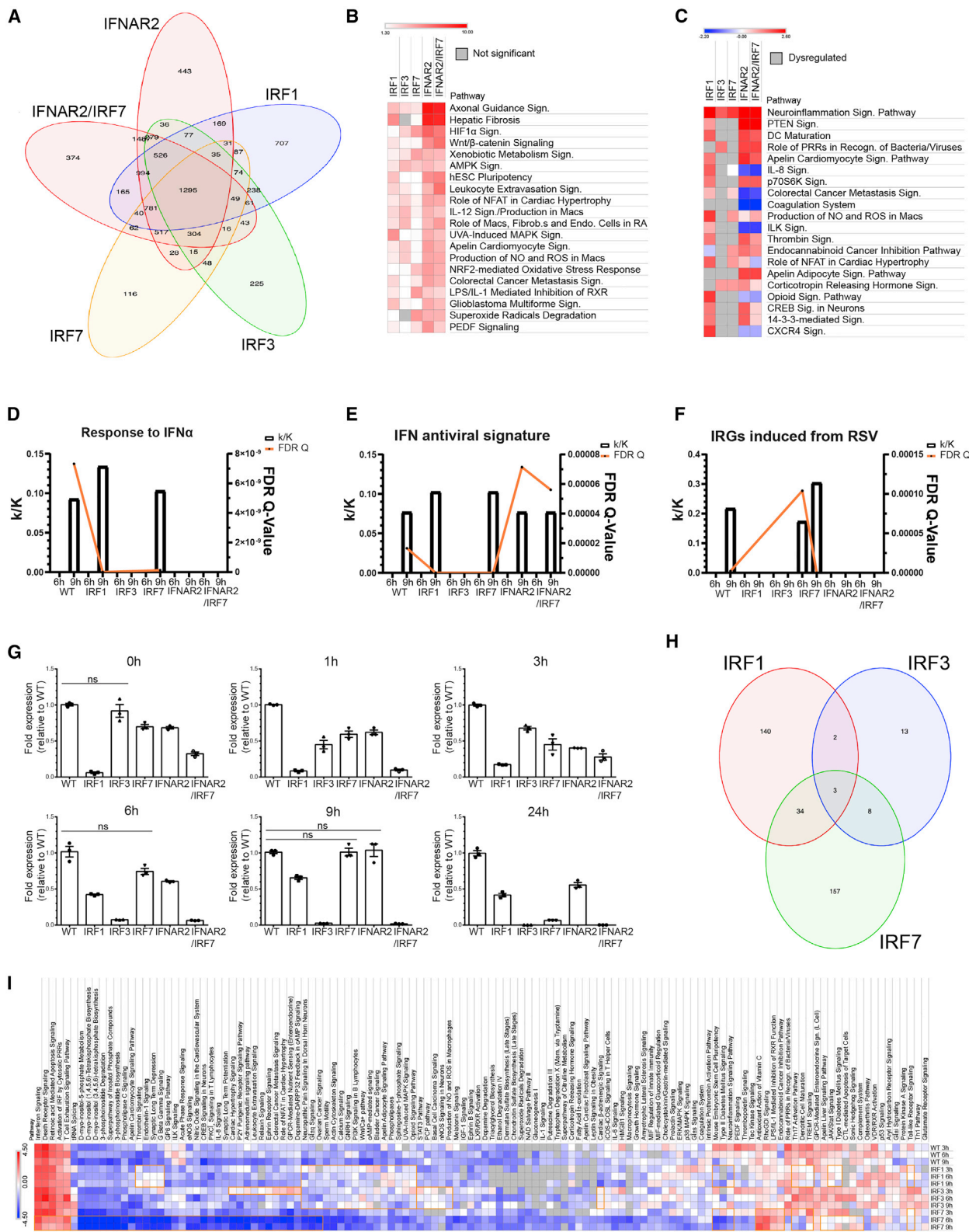
(legend on next page)

Correlation of Transcription to Total Protein Abundance

To determine the protein level dynamics of IRF regulation, cells were treated overnight, prior to quantification of total proteins by quantitative mass spectrometry. IPA revealed that although WT cells treated with high-dose IFNα upregulated IFN response proteins, only limited pathways were induced (Figure S4L; Table 1). Indeed, both IFNα and polyIC trigger a reduction in eIF2α/β/4G relative to control cells, driving global translational inhibition by the eIF2 pathway (Figure S4L; Table S4). This effect was driven by IRFs, predominantly IRF7 in response to IFN or polyIC. Removal of IRFs, particularly IRF7, consequently further drove induction of largely the same pathways observed in the transcriptomic analysis. In response to IFN or polyIC, IRF7 suppresses cholesterol biosynthesis, pyrimidine deoxyribonucleotide synthesis, MAPK/leptin/IFN/IL-/hypoxia signaling pathways, and glycolysis. This is apparently in the absence of IFN ligands, as no IFNs were detected out of ~6,000 proteins (Table S4). A degree of caution must follow this methodology, however, as predicted protein spectra do not account for post-translational modifications, potentially obscuring peptide detection. Other pathways such as cell cycle, endocytic signaling, and protein ubiquitination are significantly altered and highly dysregulated.

IRF3 and IRF7 Are Essential for Antiviral and Non-viral Pathways in Response to a Bat Orthoreovirus, PRV3M

Pteropine orthoreoviruses (PRVs) are bat viruses known to induce a potent IFN-type response in bat cells. To investigate how IRFs regulate the kinetics of PRV3M (Melaka virus), a virus known to cause zoonotic infections in humans (Chua et al., 2007; La Cruz-Rivera et al., 2017; Mok et al., 2015, 2017; Tan et al., 2017; Voon et al., 2015), transcriptome studies post-infection (MOI, 1) were used. They reveal a pro-viral role for IRF3 at early time points, with respect to viral RNA load. However, this was abrogated by 24 h (Table S5). IRF7 and IFNAR2 deficiency resulted in increased viral load at both 9 h and 24 h, yielding a 2-fold increase for IRF7 and 4-fold increase for IFNAR2 at 24 h, whereas IRF1 was significant only at late time points (Figures 5A and 5B). This finding was reflected in the plaque assays (Figure S5A). An analysis of each genome segment revealed a ubiquitous increase in viral RNA across the PRV3M genome, indicating limited interference in the transcription of

specific viral genes (Figure S5B). IRF-and IFNAR2-specific DEG analysis post-infection reveal that IRF1 had the largest effect (Figure 5C) and, yet, all three IRFs affected the amount of viral RNA.

The "IFN response" and "Death Receptor" pathways require intact IRF3/7 and IFNAR2 (Figure 5D). IRF1 deficiency enhances the IFN response. Other pathways affected by all three IRFs and IFNAR2 include oxidative phosphorylation, gluconeogenesis, and eIF2 signaling and pathways involved in sensing of NOS/ROS, which are actively downregulated. TREM1 signaling, citrulline biosynthesis, growth hormone, and TLR signaling pathways are switched on, and this is dependent on IRF1/3 and IFNAR2. The absence of IRF1 and IRF7 unexpectedly enhances p38 mitogen-activated protein kinase (MAPK), phosphatidylinositol 3-kinase (PI3K), Tec kinase, chemokine, phospholipase, ERK and VEGF signaling at the 9-h time point. IRF3 was critical for intracellular calcium, cyclic AMP (cAMP), GPCR, and intracellular phospholipid signaling pathways. IRF7 was required to turn off GPCR and phospholipase signaling later during infection, after an initial activation at 9 h.

Although the antiviral IRG geneset was robustly upregulated in both WT cells and IRF1-deficient cells, they were absent in IRF3/7/IFNAR2 KO cells (Figure 5E). However, specific genes like PARP15, UBE2L6, RNF213, and ETV7 were affected by IRF1. This result indicates that IRF7 plays a critical role early in viral infection, where it is activated in response to alternative TLR/PRR-stimulii by polyIC (Cao et al., 2008; Kawai et al., 2004; Weiss et al., 2012). Examination of "hypothetical regulators" matching the DEGs suggests IRF7 is de-activating SMARCA4, while activating multiple poorly characterized microRNAs (miRNAs) (Figure S5C). IRF3 was involved in de-activating ACKR2 while simultaneously driving a STAT1 signature of genes. Overall, the induction of the antiviral geneset (Figure 5E) correlated with infectious virus production, whereby IRF7 and IRF3 KO PakiT03 cells produced more virus, followed by IRF1, as visible by plaque assays on Vero E6 cells (Figure 5F). This finding indicates that all three IRFs contribute to the antiviral response to PRV3M and affect virus production. IRF7 sustained the antiviral geneset at later time points; however, this did not correlate with the production of IFN ligands (Figure S5D) and largely did not involve transcriptional control of known negative regulators of IFN signaling (Figure S5E). There was a mild regulation of

---

Figure 4. IRF-Regulated Genes Post-induction with polyIC or IFN

(A) Venn diagram for significantly DEGs post-treatment with polyIC (in both time points) for IRF1/3/7 CRISPR KO cells or IFNAR2 and IFNAR2/IRF7 double KO cells.

(B) Top 20 pathways that significantly affected post-polyIC induction at 6 h, compared to WT, calculated from DEG p value. Scale as indicated for −log(p value).

(C) Top 20 pathways that significantly affected post-polyIC induction, compared to WT, calculated from the DEG coefficient of correlation. Scale as indicated for Z score (amplitude of response); gray indicates dysregulated genes (in the pathway up-and downregulated).

(D) Gene set enrichment analysis (GSEA) score (k/K) for the hallmark response to IFNα-ligand geneset.

(E) As per (D) for the IFN-induced antiviral BOSCO gene signature (GSEA c3).

(F) As per (D) for the IFN-responsive gene signature post infection with (NS1-knockdown) RSV (ZHANG, GSEA c3).

(G) qPCR validation of IFIT1 expression across time (as indicated) in PakiT03 WT, IRF1/3/7, or IFNAR2/IFNAR2/IRF7 (IFNAR2/I7) double KO cells, normalized to housekeeping and graphed as fold change relative to the geometric mean of WT for the same time point. All cells are significant by unpaired, two-tailed t test compared to WT unless indicated otherwise (ns). Error bars represent SEM.

(H) DEG analysis as per (A) for IRF1/3/7 KO cells compared to WT for significant DEGs (>2-fold change, p < 0.05) in at least 2 time points post-IFNα3 treatment (3 h, 6 h, and 9 h).

(I) Heatmap of significantly activated/suppressed pathways for cells as per (H) post-treatment with IFNα3 for 3 h, 6 h, and 9 h, as calculated by IPA for genes with >2-fold change and graphed as activation Z score (scale as indicated, min/0/max). Orange box indicates highlighted regions differently regulated by IRF KO compared to WT control. Less-red compared to WT indicates the pathway is upregulated by that IRF.

Table 1. Top 15 Up- and Downregulated Proteins with Response to Treatment

WT		IRF1 KO		IRF3 KO		IRF7 KO	
IFN↑	pIC↑	IFN↑	pIC↑	IFN↑	pIC↑	IFN↑	pIC↑
OAS2	FOXG1	OAS2	DPAGT1	NAA15	TPMT	TBPL1	TBPL1
KCNA3	HDHD2	SYNPO2	SYNPO2	TBPL1	TBPL1	TPMT	CAMSAP3
BST2	QRICH1	TBPL1	FMR1	IFI6	NAA15	QTRT1	OAS3
STX3	OAS2	ISG15	FOXG1	TPMT	IFI6	FOSL1	ZBTB34
IFI6	SUPT7L	EXOC6	AQP1	S100A8	S100A8	IFI6	LY6H
LY6H	TANC1	OAS1	ARHGAP17	S100A9	TACC3	OAS3	POLR2F
SPTBN4	CLINT1	XAF1	IRAG2	OAS1	WIPF1	ZBTB34	IFI6
UBE2L6	LRSAM1	IFIT3	UBA7	WIPF1	DCXR	STX11	TRMT5
ZBTB34	ATG16L1	PCBP3	DMTN	PIR	S100A9	IFIT3	XAF1
ISG15	TICRR	NUDT12	TNFAIP2	KIF2B	RAB39B	NAA15	OASL
LGALS9	MRPL34	TNFAIP2	EXOC6	DCXR	DDX58	USP16	EEF1A2
NRF1	SPTBN4	VGLL2	MYH14	QTRT1	AZI2	TRAPPC11	IFIT3
OAS1	FMR1	INO80E	INO80E	ECD	QTRT1	POLR2F	DDX58
TICRR	TMEM168	CLDN1	OAS2	PABPC1L	ZBP1	ATM	B2M
USP18	ZBTB34	MADD	TBPL1	BST2	OAS1	SLC25A4	COMMD1
IFN↓	pIC↓	IFN↓	pIC↓	IFN↓	pIC↓	IFN↓	pIC↓
USP16	VTA1	PTPRC	PTPRC	PTPRC	LRRC7	LRRC7	LRRC7
VTA1	ACY1	C3	C3	LRRC7	PTPRC	SLC43A3	SLC43A3
ACY1	SIPA1L3	FBXO28	FBXO28	CERS4	CERS4	C3	PTPRC
MPLKIP	CIR1	IFNAR1	NOL12	XPR1	XPR1	PAN3	PAN3
SIPA1L3	DES	ERGIC1	CSRP2	PPM1E	DES	IFNAR1	C3
CIR1	RCC1L	DES	IL6ST	DES	RBP1	PTPRC	POLR1D
HOXA5	INO80E	CSRP2	MATN3	RBP1	PPM1E	RASAL2	MRPS34
TMEM132A	LAMB2	AMFR	ZBTB14	MYO5C	NUDT12	MRPS34	IFNAR1
WAC	RABL6	ZBTB14	DES	YIF1A	YIF1A	MAN2A1	RASAL2
PTER	TMEM132A	ZC3H8	ERGIC1	ING5	ING5	GIT2	RBM15B
RCC1L	UBAC1	CERS4	GGT7	NUDT12	TICRR	POLR1D	ZC3H8
SAP130	CIC	MATN3	ZC3H8	LRP10	MYO5C	XPR1	GIT2
RABL6	THBS2	IL6ST	ARHGAP21	TMEM35A	PCLO	CEP290	BRI3BP
SESN2	ATM	LOXL4	AMFR	PCLO	SPATA1	RBM15B	XPR1
DOP1B	PTER	LRRC8A	ARSI	TAF1	PEX5	ZC3H8	CEP290

TRIM21 and USP18 by IRF3/7, although this is likely IFN dependent. IFNβ expression, most significantly changed in IRF3/7 KO cells, was induced by 9 h in IRF1-deficient cells, although this failed to induce the typical antiviral gene signature. The overall amplitude of IFN-ligand induction was quite low (Figure S5D) compared to a potent induction of IRGs (Figure 5E; Table S5). IRF3/7 did contribute to higher levels of STAT1/STAT2/IRF9 at late time points, which may contribute to IFN-ligand IFN-independent signaling (Blaszczyk et al., 2015; Cheon et al., 2013; Nan et al., 2018; Sung et al., 2015), Although their induction was not observed in the absence of IFNAR2. The absence of classical antiviral IRG expression in IRF3/7 or IFNAR2 deficiency highlights the need for both intact IFN signaling and IRF-directed gene expression for the classical response. Multiple signaling pathways (e.g., mTOR, Sirtuin, PPAR, LXR, antioxidant, and RhoGDi) are observed to be IFN-signaling independent and, yet, regulated by IRFs.

Reconstitution Alleviates IRF Deficiency

To ensure specificity of the clonal cell lines chosen, reconstitution of the relevant IRF KO cell line by overexpression of IRF1/3/7-GFP fusion constructs was performed to restore antiviral protection. Titration of viral supernatants confirms that the defect in each cell line was due to the absence of IRFs and not a clonal-line-compensatory mechanism (Figure 5G). Reconstitution of IRF1/3 and 7 significantly drove an antiviral effect and reduced PRV3M production. IRF7 reconstitution was also used to drive an antiviral phenotype in IFNAR2 KO cells, IFNAR2/IRF7 double KO cells, and an IRF1/IRF7 double KO clonal cell line (Figure S5F). This indicates that *P. alecto* IRF7 alone can suppress virus production in the absence type-I IFN signaling. This phenotype can be partially observed across species with *P. alecto* IRF7 functioning in *Myotis davidii* MdKi cells to suppress virus production, despite only minimal transfection efficiency (Figure S5G).
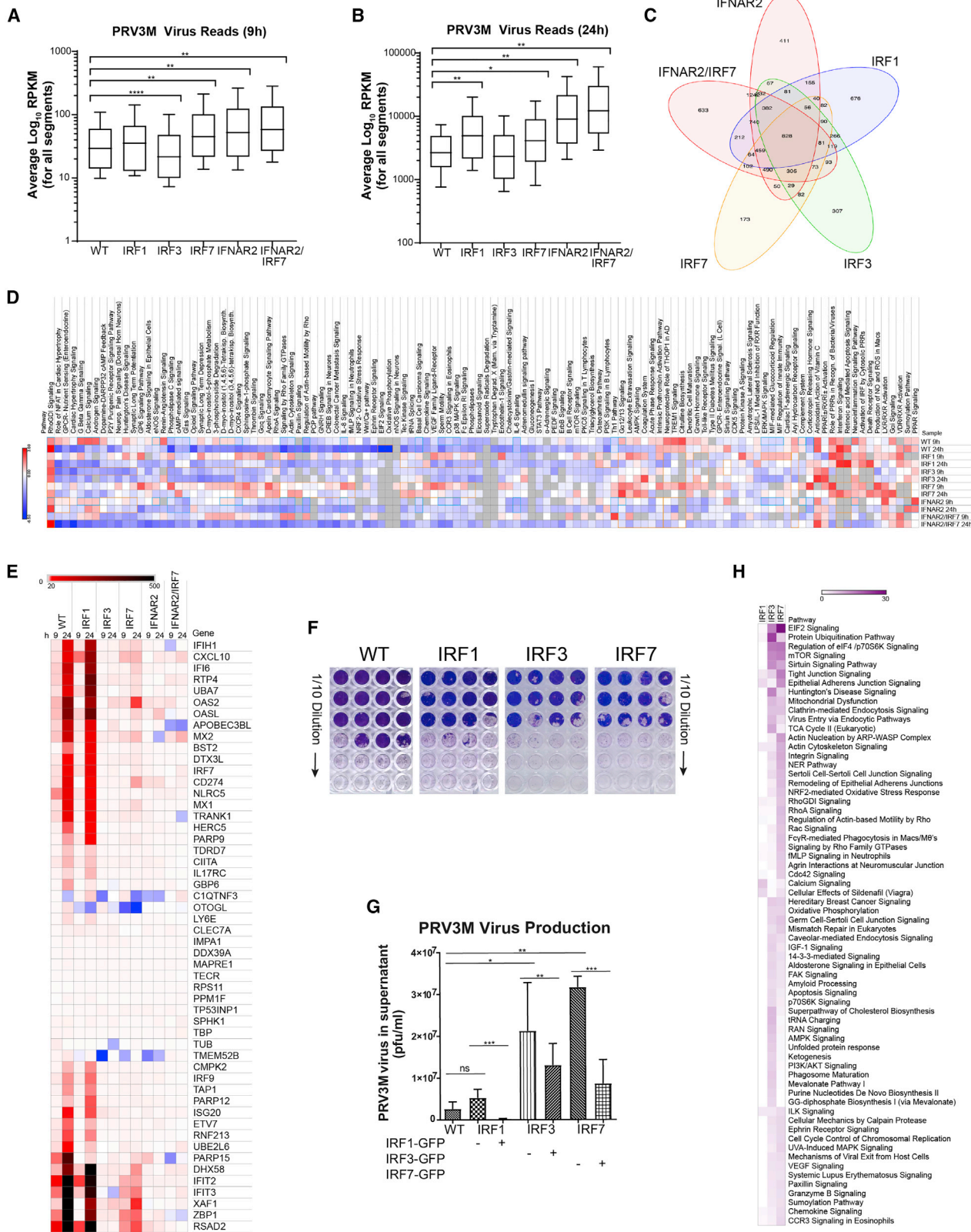
(legend on next page)

A similar trend was observed for overexpression in HEK293T human cells (Figure S5H).

DISCUSSION

Using multiple assays in bat cell lines, we show that the high-baseline IFN-like signature in bat cells is further upregulated upon dsRNA treatment in a partially IFN-signaling-independent manner. IRFs, the master regulators of IRG responses, are also highly expressed across multiple tissues. This signature is confirmed across the spleen, liver, and lung tissues in two distant species, implicating the importance of this for innate defense mechanisms in bats. Intriguingly, IRF1/7 expression is reduced in the bat's heart tissue, suggesting a lack of immune activation in the bat's heart may be important for its physiology. Although there may be significant variation due to species diversity, a recent preprint for a bat single-cell atlas of *Rhinolophus sinicus* (Ren et al., 2020) suggests comparable IRF1/3/7 expression, with RNA expression observed across both lymphoid and non-lymphoid tissue, matching our own observations. Although healthy wild-born bats with no known current infections were used, compared to seemingly healthy humans and mice, temporary housing and handling may impact the natural microbiota and alter gene expression to some degree. Similarly, the previous infection history and microbiota status of the humans compared are also unknown.

Overexpression of IRFs induces low-level type I IFNs, with IRF1 being a more potent inducer than IRF7 in direct promoter assays. Additional IRGs were upregulated by IRF1/3/7, indicating basal regulation of IRG subsets by IRF1 and IRF7 in the absence of additional stimuli. This was confirmed by nuclear localization of IRF1/7 but not IRF3, prior to dsRNA/polyIC treatment. Whether bat IRF7 has unique basal-activation properties would require further investigation, ideally across multiple bat species. IRF3-induced genes were also largely dependent on dsRNA induction, consistent with the function of its human homolog. However, early time points also indicate IRF3-dependent and IFN-ligand-independent gene induction.

Generation of CRISPR KO cells deficient in IRF1/3/7 showed IRF1 has an antiviral role in HSV infection. An IRF1 phenotype has been previously implicated in human cells (Xie et al., 2018). We demonstrate that IRF3 is important for MERS-CoV activation of innate immunity in bat cells, as expected. Unexpectedly, both

IRF1 and IRF7 also play key roles in MERS-CoV infection. IAV shows IRF1, 3, and 7 contribute equally to reducing IAV RNA in infected cells. Based on IRF TF expression in the lung, this suggests that all three IRFs regulate the dynamics of infection. Although this may be a common response feature, further investigation is needed to see if it is true for other RNA viruses and for other β-CoVs, such as SARS-CoV-2. Deeper investigation into the transcriptomic studies reveals unique and overlapping IRF-regulated genes in the basal state, without stimuli or IFN ligand. While IRF-directed gene expression has been observed in other mammals it has been studied in the context of foreign RNA for activation. One study in hematopoietic stem cells suggests that IRF7 may control basal expression patterns, although few other studies have examined this scenario directly (Eggenberger et al., 2019). The key role for IRF7 in early time points appears to contrast that of human studies for which it is believed to play a role in amplification of an antiviral response rather than in primary detection and signaling.

Despite the minimal induction of type-I IFN ligands by IFN, polyIC, or virus, various IRGs known to inhibit viruses were regulated by IRF1 (IFIT2, CIITA, CXCL10, IFIT1, UBA7, CLEC7A, PLSCR1, CCL2, CYP1b1, CD274, PARP10, OAS3, RTP4, and BST2) or IRF7 (CIITA, CD274, MX1/2, B2M, CYP1b1, IFIH1, OAS2, and IFNL1). Genes such as PARP15, TRANK1, ZBP1, and APOBEC3BL are regulated by IRF7 in an IFN-independent manner and are further amplified with intact IFN signaling. Cells with intact IRF3 and IFNAR2 still required IRF7 to mount a full response. This result also highlights dynamic differences between basal expression and overexpression studies. Many of these pathways were consistently activated post-stimulation and suggests that IRF1 regulation is critical at early time points, which is likely IFN independent, whereas IRF7 regulation occurs at both early and later time points and is critical for the response to PRV3M infection. There were clear differences in responsiveness to synthetic dsRNA compared to IFN and live virus. This fits with previous literature in bat cells suggesting unique IFN-stimulated genes, dsRNA-induced genes, and virus-induced genes that, although partially overlapping, also have unique profiles. Both findings also support a previous report of temporal differences in IRG activation in bat cells (La Cruz-Rivera et al., 2017). Type-I IFNs are expressed basally (particularly IFNω2-like) and require both IRF1 and 7. IFN induction was limited after stimulation, however, compared to the potent induction of IRGs,

---

Figure 5. Regulation of the Antiviral Response to Melaka Virus by IRF1, 3, and 7

(A) PRV3M (Melaka virus) RNA load as measured by NGS transcriptome mean FPKM (all segments) at 9 h post-infection with an MOI of 1 (washed, 3 h post-infection). Cell lines as indicated including WT, IRF1/3/7, IFNAR2, and IFNAR2/IRF7 double CRISPR KO cells.

(B) As per (A) at 24-h time point.

(C) Venn diagram of overlapping and unique DEG analysis, compared to WT, from EdgeR in both time points after infection with PRV3M for cell lines as per (A).

(D) IPA of significantly changed genes (>2-fold change, p < 0.05) compared to untreated for all cell lines as per (A) (scale as indicated, fold-change, min/max). Orange boxes highlight differences between WT and IRF clones. Blue boxes highlight similarities between WT and IFNAR2 KO cells (IFN independent).

(E) Heatmap of fold-change post-infection compared to untreated cells for the antiviral IRG subset, normalized to geometric mean of 13 housekeeping genes. A 4-color non-linear scale is used from blue-white-red-black (−1, unchanged), 20, 300-fold induction), as indicated.

(F) Viral titration on Vero E6 cells from supernatant 72 h post-infection with PRV3M at an MOI of 1; clonal cell line as indicated. Dilution series as indicated, in quadruplicate. Gaps in the monolayer occur from syncytia formation whereby syncytia are counted as a single plaque.

(G) Quantitation of viral production from titrated supernatants as per (F), including IRF1/3/7 KO cells restored with IRF1/3/7-GFP fusions constructs, respectively.

(H) IPA for the significant IP hits enriched above GFP control, expressed as p value for significance of the pathway; −log(p value), scale as indicated. Significance valeus for (A), (B), and (G) were determined by unpaired t test; ***p < 0.01, **p < 0.02, *p < 0.05 (n ≥ 3). All error bars are indicated as SEM.

suggesting negative regulation of IFN transcription. Known inhibitors of IFN signaling were not induced early in WT cells when some limited transcription was observed. Late time points suggest TRIM21, RBCK1, USP18/25, NMI, and OASL may partially contribute in this regard. The apparent shutdown of protein translation in WT cells stimulated with IFN polyIC overnight suggests a mechanism to prevent excessive immune responses or to block excessive cytokine production. This phenomenon for skewing protein translation preferentially toward IRGs has been observed previously (Chitrakar et al., 2019), although further investigation is required to see if such is the case.

IRF7-deficient cells also failed to induce a proper antiviral IRG response post-infection with PRV3M. The large increase in virus production of IRF7 KO cells, with IRF3 and IFN signaling intact, suggests IRF3 and consequent IFN induction are not capable of a complete antiviral response against PRV3M. Most non-immune cells in mammals express minimal IRF7 and rely on IRF3 to detect viral RNAs. Combined with the strong antiviral effect of IRF7 in IFNAR2 KO cells, this suggests that the additional antiviral functions of the widely distributed IRF7 are essential for mounting a complete antiviral response in bats. This may be related to IRF7's requirement to sustain IRG induction at later time points and may involve modulation of the initiation of protein translation. As IFNα1,4/ω2 ligands were still induced in IRF7-deficient cells, it is not likely to be due to the decreased IFNβ expression. The role of IRF7 at late time points possibly involves suppression of cAMP, p38/MAPK, AMPK, and GPCR/phospholipase signaling (the most significantly affected pathways). This supports our finding that IRF7 is a potent antiviral for PRV3M viral load/infectious titer, which can be conferred by *P. alecto* IRF7 overexpression in multiple species/cell types.

Many of these bat-specific, IRF-regulated genes contribute to pathways such as metabolism, glycolysis, intracellular lipids, GPCR, tryptophan metabolism, and ROS/NO signaling. As the master regulators of the immune system, IRFs are considered essential for the efficient development of immune cells. These pathways also suggest a deeper regulation of cell biology that may contribute to an IRF-regulated antiviral state in addition to the typical IFN-like signatures. Metabolism and ROS particularly are important for trained immunity. For example, IRF1 contributes to SMAD2 expression that may affect STAT3/IFNγ target genes and Th17/Treg development. The restriction on IFN production may also play a role in the development of immune cells and has been implicated previously for B cells, T cells, and monocytes (Gabriele et al., 2004; Kavrochorianou et al., 2016; Silva-Barrios et al., 2016). IRF7 plays a role in microglia polarization (Tanaka et al., 2015), IRF1 in training macrophage responses (Cheng et al., 2019; Langlais et al., 2016), and both in PRR signaling in dendritic cells (Cohen et al., 2014; Honda et al., 2005; Hu et al., 2008; Li et al., 2014b; Robertson et al., 2014; Weiss et al., 2012); further investigations are warranted to examine the role for IRFs in immune cell development in bats.

In summary, both IRF1 and IRF7 regulate IFNs and basal expression of antiviral genes in *P. alecto* bats. IRF1/3/7 regulate genes at early time points independent of significant IFN induction, as opposed to primarily IRF3 in humans. Many of the IRF-regulated genes/pathways were not previously revealed in studies of IRF induction in humans/mice. Using dsRNA and an RNA virus, we highlight the importance of IRF3 and 7 post-induction. We demonstrate that bat cells have a prolonged IFN-like antiviral signature even in the absence of IFN ligands, which are minimally induced during early infection. Although careful examination of IRF master regulation will be needed across the numerous bat species and *in vivo*, given the unique tolerance of infection observed in bats, this study highlights IFN-, dsRNA-, and virus-induced genes and pathways not previously highlighted in other mammals. The higher basal expression of IRFs may contribute to this suppression and regulates HSV-1, IAV, MERS-CoV, and PRV3M infection, even in the absence of type I IFNs. This potentially influences the host's ability to serve as a zoonotic reservoir and tolerance for viral infection. This work highlights key areas to focus on in not only bat innate immunity but also protection against viruses in other mammalian species. It also highlights the need for studying the conditions required for IRF1/7 expression in humans, post-viral infection, and any potential to alter their regulation.

STAR★METHODS

Detailed methods are provided in the online version of this paper and include the following:

- KEY RESOURCES TABLE
- RESOURCE AVAILABILITY
  - Lead Contact
  - Materials Availability
  - Data and Code Availability
- EXPERIMENTAL MODEL AND SUBJECT DETAILS
  - Animals, viruses and cells
- METHOD DETAILS
  - RNA extraction and quantitative RT-PCR
  - RNaseq analysis
  - Viral plaque/titration assays
  - Viral infection/ligand stimulation assays
  - Mass spectrometry analysis
  - MS-data analysis
  - CRISPR Knockout cell line generation
  - IRF overexpression and luciferase studies
  - Pathway analysis
- QUANTIFICATION AND STATISTICAL ANALYSIS

REFERENCES

Anders, S., Pyl, P.T., and Huber, W. (2015). HTSeq—a Python framework to work with high-throughput sequencing data. Bioinformatics *31*, 166–169.

Andrilenas, K.K., Ramlall, V., Kurland, J., Leung, B., Harbaugh, A.G., and Siggers, T. (2018). DNA-binding landscape of IRF3, IRF5 and IRF7 dimers: implications for dimer-specific gene regulation. Nucleic Acids Res. *46*, 2509–2520.

Ashley, C.L., Abendroth, A., McSharry, B.P., and Slobedman, B. (2019). Interferon-Independent Upregulation of Interferon-Stimulated Genes during Human Cytomegalovirus Infection is Dependent on IRF3 Expression. Viruses *11*, 246.

Austad, S.N., and Fischer, K.E. (1991). Mammalian aging, metabolism, and ecology: Evidence from the bats and marsupials. J. Gerontol. *46*, B47–B53.

Baker, M.L., Schountz, T., and Wang, L.F. (2013). Antiviral immune responses of bats: a review. Zoonoses Public Health *60*, 104–116.

Banerjee, A., Falzarano, D., Rapin, N., Lew, J., and Misra, V. (2019). Interferon Regulatory Factor 3-Mediated Signaling Limits Middle-East Respiratory Syndrome (MERS) Coronavirus Propagation in Cells from an Insectivorous Bat. Viruses *11*, 152.

Barnes, B.J., Richards, J., Mancl, M., Hanash, S., Beretta, L., and Pitha, P.M. (2004). Global and distinct targets of IRF-5 and IRF-7 during innate response to viral infection. J. Biol. Chem. *279*, 45194–45207.

Blaszczyk, K., Olejnik, A., Nowicka, H., Ozgyin, L., Chen, Y.-L., Chmielewski, S., Kostyrko, K., Wesoly, J., Balint, B.L., Lee, C.-K., and Bluyssen, H.A. (2015). STAT2/IRF9 directs a prolonged ISGF3-like transcriptional response and antiviral activity in the absence of STAT1. Biochem. J. *466*, 511–524.

Bouma, H.R., Carey, H.V., and Kroese, F.G.M. (2010). Hibernation: the immune system at rest? J. Leukoc. Biol. *88*, 619–624.

Brunet-Rossinni, A.K. (2004). Reduced free-radical production and extreme longevity in the little brown bat (Myotis lucifugus) versus two non-flying mammals. Mech. Ageing Dev. *125*, 11–20.

Brunet Rossinni, A.K. (2004). Testing the free radical theory of aging in bats. Ann. N Y Acad. Sci. *1019*, 506–508.

Cabrera-Romo, S., Recio-Tótoro, B., Alcalá, A.C., Lanz, H., del Ángel, R.M., Sánchez-Cordero, V., Rodríguez-Moreno, Á., and Ludert, J.E. (2014). Experimental inoculation of Artibeus jamaicensis bats with dengue virus serotypes 1 or 4 showed no evidence of sustained replication. Am. J. Trop. Med. Hyg. *91*, 1227–1234.

Cao, W., Manicassamy, S., Tang, H., Kasturi, S.P., Pirani, A., Murthy, N., and Pulendran, B. (2008). Toll-like receptor-mediated induction of type I interferon in plasmacytoid dendritic cells requires the rapamycin-sensitive PI(3)K-mTOR-p70S6K pathway. Nat. Immunol. *9*, 1157–1164.

Caracausi, M., Piovesan, A., Antonaros, F., Strippoli, P., Vitale, L., and Pelleri, M.C. (2017). Systematic identification of human housekeeping genes possibly useful as references in gene expression studies. Mol. Med. Rep. *16*, 2397–2410.

Cheng, Q., Behzadi, F., Sen, S., Ohta, S., Spreafico, R., Teles, R., Modlin, R.L., and Hoffmann, A. (2019). Sequential conditioning-stimulation reveals distinct gene- and stimulus-specific effects of Type I and II IFN on human macrophage functions. Sci. Rep. *9*, 5288.

Cheon, H., Holvey-Bates, E.G., Schoggins, J.W., Forster, S., Hertzog, P., Imanaka, N., Rice, C.M., Jackson, M.W., Junk, D.J., and Stark, G.R. (2013). IFNβ-dependent increases in STAT1, STAT2, and IRF9 mediate resistance to viruses and DNA damage. EMBO J. *32*, 2751–2763.

Chitrakar, A., Rath, S., Donovan, J., Demarest, K., Li, Y., Sridhar, R.R., Weiss, S.R., Kotenko, S.V., Wingreen, N.S., and Korennykh, A. (2019). Real-time 2-5A kinetics suggest that interferons β and λ evade global arrest of translation by RNase L. Proc. Natl. Acad. Sci. USA *116*, 2103–2111.

Chua, K.B., Crameri, G., Hyatt, A., Yu, M., Tompang, M.R., Rosli, J., McEachern, J., Crameri, S., Kumarasamy, V., Eaton, B.T., and Wang, L.F. (2007). A previously unknown reovirus of bat origin is associated with an acute respiratory disease in humans. Proc. Natl. Acad. Sci. USA *104*, 11424–11429.

Cohen, M., Matcovitch, O., David, E., Barnett-Itzhaki, Z., Keren-Shaul, H., Blecher-Gonen, R., Jaitin, D.A., Sica, A., Amit, I., and Schwartz, M. (2014). Chronic exposure to TGFβ1 regulates myeloid cell inflammatory response in an IRF7-dependent manner. EMBO J. *33*, 2906–2921.

Crameri, G., Todd, S., Grimley, S., McEachern, J.A., Marsh, G.A., Smith, C., Tachedjian, M., De Jong, C., Virtue, E.R., Yu, M., et al. (2009). Establishment, immortalisation and characterisation of pteropid bat cell lines. PLoS One *4*, e8266.

La Cruz-Rivera, P.C.D., Kanchwala, M., Liang, H., Kumar, A., Wang, L.-F., Xing, C., and Schoggins, J.W. (2017). The IFN response in bat cells consists of canonical and non-canonical ISGs with unique temporal expression kinetics. bioRxiv. https://doi.org/10.1101/167999.

Currie, S.E., Stawski, C., and Geiser, F. (2018). Cold-hearted bats: uncoupling of heart rate and metabolism during torpor at sub-zero temperatures. J. Exp. Biol. *221*, jeb170894.

Davis, A., Bunning, M., Gordy, P., Panella, N., Blitvich, B., and Bowen, R. (2005). Experimental and natural infection of North American bats with West Nile virus. Am. J. Trop. Med. Hyg. *73*, 467–469.

Dery, K.J., Silver, C., Yang, L., and Shively, J.E. (2018). Interferon regulatory factor 1 and a variant of heterogeneous nuclear ribonucleoprotein L coordinately silence the gene for adhesion protein CEACAM1. J. Biol. Chem. *293*, 9277–9291.

Eggenberger, J., Blanco-Melo, D., Panis, M., Brennand, K.J., and tenOever, B.R. (2019). Type I interferon response impairs differentiation potential of pluripotent stem cells. Proc. Natl. Acad. Sci. USA *116*, 1384–1393.

Eisenberg, E., and Levanon, E.Y. (2013). Human housekeeping genes, revisited. Trends Genet. *29*, 569–574.

Foley, N.M., Hughes, G.M., Huang, Z., Clarke, M., Jebb, D., Whelan, C.V., Petit, E.J., Touzalin, F., Farcy, O., Jones, G., et al. (2018). Growing old, yet staying young: The role of telomeres in bats' exceptional longevity. Sci. Adv. *4*, eaao0926.

Fuchs, J., Hölzer, M., Schilling, M., Patzina, C., Schoen, A., Hoenen, T., Zimmer, G., Marz, M., Weber, F., Müller, M.A., et al. (2017). Evolution and antiviral specificity of interferon-induced Mx proteins of bats against Ebola-, Influenza-, and other RNA viruses. J. Virol. *91*, e00361-17.

Gabriele, L., Borghi, P., Rozera, C., Sestili, P., Andreotti, M., Guarini, A., Montefusco, E., Foà, R., and Belardelli, F. (2004). IFN-α promotes the rapid differentiation of monocytes from patients with chronic myeloid leukemia into

activated dendritic cells tuned to undergo full maturation after LPS treatment. Blood *103*, 980–987.

Garvin, A.J., Khalaf, A.H.A., Rettino, A., Xicluna, J., Butler, L., Morris, J.R., Heery, D.M., and Clarke, N.M. (2019). GSK3β-SCFFBXW7α mediated phosphorylation and ubiquitination of IRF1 are required for its transcription-dependent turnover. Nucleic Acids Res. *47*, 4476–4494.

Génin, P., Vaccaro, A., and Civas, A. (2009). The role of differential expression of human interferon–a genes in antiviral immunity. Cytokine Growth Factor Rev. *20*, 283–295.

Ghosh, S., and Chan, C.-K.K. (2016). Analysis of RNA-Seq Data Using TopHat and Cufflinks (Humana Press), pp. 339–361.

Glennon, N.B., Jabado, O., Lo, M.K., and Shaw, M.L. (2015). Transcriptome Profiling of the Virus-Induced Innate Immune Response in Pteropus vampyrus and Its Attenuation by Nipah Virus Interferon Antagonist Functions. J. Virol. *89*, 7550–7566.

Han, Y., Zheng, G., Yang, T., Zhang, S., Dong, D., and Pan, Y.H. (2015). Adaptation of peroxisome proliferator-activated receptor alpha to hibernation in bats. BMC Evol. Biol. *15*, 88.

Herbold, J.R., Heuschele, W.P., Berry, R.L., and Parsons, M.A. (1983). Reservoir of St. Louis encephalitis virus in Ohio bats. Am. J. Vet. Res. *44*, 1889–1893.

Hölzer, M., Schoen, A., Wulle, J., Müller, M.A., Drosten, C., Marz, M., and Weber, F. (2019). Virus- and Interferon Alpha-Induced Transcriptomes of Cells from the Microbat Myotis daubentonii. iScience *19*, 647–661.

Honda, K., Yanai, H., Negishi, H., Asagiri, M., Sato, M., Mizutani, T., Shimada, N., Ohba, Y., Takaoka, A., Yoshida, N., and Taniguchi, T. (2005). IRF-7 is the master regulator of type-I interferon-dependent immune responses. Nature *434*, 772–777.

Hu, Y., Park-Min, K.-H., Yarilina, A., and Ivashkiv, L.B. (2008). Regulation of STAT pathways and IRF1 during human dendritic cell maturation by TNF-alpha and PGE2. J. Leukoc. Biol. *84*, 1353–1360.

Huang, Z., Jebb, D., and Teeling, E.C. (2016). Blood miRNomes and transcriptomes reveal novel longevity mechanisms in the long-lived bat, Myotis myotis. BMC Genomics *17*, 906.

Irving, A.T., Wang, D., Vasilevski, O., Latchoumanin, O., Kozer, N., Clayton, A.H.A., Szczepny, A., Morimoto, H., Xu, D., Williams, B.R.G., and Sadler, A.J. (2012). Regulation of actin dynamics by protein kinase R control of gelsolin enforces basal innate immune defense. Immunity *36*, 795–806.

Irving, A.T., Ng, J.H.J., Boyd, V., Dutertre, C.A., Ginhoux, F., Dekkers, M.H., Meers, J., Field, H.E., Crameri, G., and Wang, L.-F. (2019). Optimizing dissection, sample collection and cell isolation protocols for frugivorous bats. Methods Ecol. Evol. *11*, 150–158.

Irving, A.T., Rozario, P., Kong, P.S., Luko, K., Gorman, J.J., Hastie, M.L., Chia, W.N., Mani, S., Lee, B.P.H., Smith, G.J.D., et al. (2020). Robust dengue virus infection in bat cells and limited innate immune responses coupled with positive serology from bats in IndoMalaya and Australasia. Cell. Mol. Life Sci. *77*, 1607–1622.

Jones, M.E.B., Schuh, A.J., Amman, B.R., Sealy, T.K., Zaki, S.R., Nichol, S.T., and Towner, J.S. (2015). Experimental Inoculation of Egyptian Rousette Bats (Rousettus aegyptiacus) with Viruses of the Ebolavirus and Marburgvirus Genera. Viruses *7*, 3420–3442.

Jones, M.E.B., Amman, B.R., Sealy, T.K., Uebelhoer, L.S., Schuh, A.J., Flietstra, T., Bird, B.H., Coleman-McCray, J.D., Zaki, S.R., Nichol, S.T., and Towner, J.S. (2019). Clinical, Histopathologic, and Immunohistochemical Characterization of Experimental Marburg Virus Infection in A Natural Reservoir Host, the Egyptian Rousette Bat (*Rousettus aegyptiacus*). Viruses *11*, 214.

Kavrochorianou, N., Evangelidou, M., Markogiannaki, M., Tovey, M., Thyphronitis, G., and Haralambous, S. (2016). IFNAR signaling directly modulates T lymphocyte activity, resulting in milder experimental autoimmune encephalomyelitis development. J. Leukoc. Biol. *99*, 175–188.

Kawai, T., Sato, S., Ishii, K.J., Coban, C., Hemmi, H., Yamamoto, M., Terai, K., Matsuda, M., Inoue, J., Uematsu, S., et al. (2004). Interferon-α induction

through Toll-like receptors involves a direct interaction of IRF7 with MyD88 and TRAF6. Nat. Immunol. *5*, 1061–1068.

Kuleshov, M.V., Jones, M.R., Rouillard, A.D., Fernandez, N.F., Duan, Q., Wang, Z., Koplev, S., Jenkins, S.L., Jagodnik, K.M., Lachmann, A., et al. (2016). Enrichr: a comprehensive gene set enrichment analysis web server 2016 update. Nucleic Acids Res. *44*, W90–W97.

Langlais, D., Barreiro, L.B., and Gros, P. (2016). The macrophage IRF8/IRF1 regulome is required for protection against infections and is associated with chronic inflammation. J. Exp. Med. *213*, 585–603.

Law, C.W., Alhamdoosh, M., Su, S., Dong, X., Tian, L., Smyth, G.K., and Ritchie, M.E. (2016). RNA-seq analysis is easy as 1-2-3 with limma, Glimma and edgeR. F1000Res. *5*, 1408.

Li, B., and Dewey, C.N. (2011). RSEM: accurate transcript quantification from RNA-Seq data with or without a reference genome. BMC Bioinformatics *12*, 323.

Li, W., Hofer, M.J., Jung, S.R., Lim, S.-L., and Campbell, I.L. (2014a). IRF7-dependent type I interferon production induces lethal immune-mediated disease in STAT1 knockout mice infected with lymphocytic choriomeningitis virus. J. Virol. *88*, 7578–7588.

Li, Y.-F., Lee, K.-G., Ou, X., and Lam, K.-P. (2014b). Bruton's tyrosine kinase and protein kinase C μ are required for TLR7/9-induced IKKα and IRF-1 activation and interferon-β production in conventional dendritic cells. PLoS One *9*, e105420.

Liang, Y.Z., Wu, L.J., Zhang, Q., Zhou, P., Wang, M.N., Yang, X.L., Ge, X.Y., Wang, L.F., and Shi, Z.L. (2015). Cloning, expression, and antiviral activity of interferon β from the Chinese microbat, Myotis davidii. Virol. Sin. *30*, 425–432.

Lin, R., and Hiscott, J. (1999). A role for casein kinase II phosphorylation in the regulation of IRF-1 transcriptional activity. Mol. Cell. Biochem. *191*, 169–180.

Lin, R., Mamane, Y., and Hiscott, J. (2000a). Multiple regulatory domains control IRF-7 activity in response to virus infection. J. Biol. Chem. *275*, 34320–34327.

Lin, R., Génin, P., Mamane, Y., and Hiscott, J. (2000b). Selective DNA binding and association with the CREB binding protein coactivator contribute to differential activation of alpha/beta interferon genes by interferon regulatory factors 3 and 7. Mol. Cell. Biol. *20*, 6342–6353.

McNab, B.K. (1989). Temperature Regulation and Rate of Metabolism in Three Bornean Bats. J. Mammal. *70*, 153–161.

Middleton, D.J., Morrissy, C.J., van der Heide, B.M., Russell, G.M., Braun, M.A., Westbury, H.A., Halpin, K., and Daniels, P.W. (2007). Experimental Nipah virus infection in pteropid bats (Pteropus poliocephalus). J. Comp. Pathol. *136*, 266–272.

Mok, L., Wynne, J.W., Grimley, S., Shiell, B., Green, D., Monaghan, P., Pallister, J., Bacic, A., and Michalski, W.P. (2015). Mouse fibroblast L929 cells are less permissive to infection by Nelson Bay orthoreovirus compared to other mammalian cell lines. J. Gen. Virol. *96*, 1787–1794.

Mok, L., Wynne, J.W., Tachedjian, M., Shiell, B., Ford, K., Matthews, D.A., Bacic, A., and Michalski, W.P. (2017). Proteomics informed by transcriptomics for characterising differential cellular susceptibility to Nelson Bay orthoreovirus infection. BMC Genomics *18*, 615.

Nan, J., Wang, Y., Yang, J., and Stark, G.R. (2018). IRF9 and unphosphorylated STAT2 cooperate with NF-κB to drive IL6 expression. Proc. Natl. Acad. Sci. USA *115*, 3906–3911.

O'Mara, M.T., Wikelski, M., Voigt, C.C., Ter Maat, A., Pollock, H.S., Burness, G., Desantis, L.M., and Dechmann, D.K. (2017). Cyclic bouts of extreme bradycardia counteract the high metabolism of frugivorous bats. eLife *6*, e26686.

Obregón-Morales, C., Aguilar-Setién, Á., Perea Martínez, L., Galvez-Romero, G., Martínez-Martínez, F.O., and Aréchiga-Ceballos, N. (2017). Experimental infection of Artibeus intermedius with a vampire bat rabies virus. Comp. Immunol. Microbiol. Infect. Dis. *52*, 43–47.

Pavlovich, S.S., Lovett, S.P., Koroleva, G., Guito, J.C., Arnold, C.E., Nagle, E.R., Kulcsar, K., Lee, A., Thibaud-Nissen, F., Hume, A.J., et al. (2018). The

Egyptian Rousette Genome Reveals Unexpected Features of Bat Antiviral Immunity. Cell *173*, 1098–1110.e18.

Paweska, J.T., Storm, N., Grobbelaar, A.A., Markotter, W., Kemp, A., and Jansen van Vuren, P. (2016). Experimental Inoculation of Egyptian Fruit Bats (Rousettus aegyptiacus) with Ebola Virus. Viruses *8*, 29.

Perea-Martínez, L., Moreno-Sandoval, H.N., Moreno-Altamirano, M.M., Salas-Rojas, M., García-Flores, M.M., Aréchiga-Ceballos, N., Tordo, N., Marianneau, P., and Aguilar-Setién, A. (2013). Experimental infection of Artibeus intermedius bats with serotype-2 dengue virus. Comp. Immunol. Microbiol. Infect. Dis. *36*, 193–198.

Piya, S., and Kim, T.-H. (2018). The Effect of Lipopolysaccharide on Noxa Expression Is Mediated through IRF1, 3, and 7. J. Microbiol. Biotechnol. *28*, 491–497.

Podlutsky, A.J., Khritankov, A.M., Ovodov, N.D., and Austad, S.N. (2005). A new field record for bat longevity. J. Gerontol. A Biol. Sci. Med. Sci. *60*, 1366–1368.

Reagan, R., and Brueckner, A.L. (1952). Studies of dengue fever virus in the cave bat (Myotus lucifugus). J. Infect. Dis. *91*, 145–146.

Ren, L., Wu, C., Guo, L., Yao, J., Wang, C., Xiao, Y., Pisco, A.O., Wu, Z., Lei, X., Liu, Y., et al. (2020). Single-cell transcriptional atlas of the Chinese horseshoe bat (Rhinolophus sinicus) provides insight into the cellular mechanisms which enable bats to be viral reservoirs. bioRxiv, 2020.06.30.175778.

Robertson, S.J., Lubick, K.J., Freedman, B.A., Carmody, A.B., and Best, S.M. (2014). Tick-borne flaviviruses antagonize both IRF-1 and type I IFN signaling to inhibit dendritic cell function. J. Immunol. *192*, 2744–2755.

Robinson, M.D., McCarthy, D.J., and Smyth, G.K. (2010). edgeR: a Bioconductor package for differential expression analysis of digital gene expression data. Bioinformatics *26*, 139–140.

Schmid, S., Mordstein, M., Kochs, G., García-Sastre, A., and Tenoever, B.R. (2010). Transcription factor redundancy ensures induction of the antiviral state. J. Biol. Chem. *285*, 42013–42022.

Schoggins, J.W., and Rice, C.M. (2011). Interferon-stimulated genes and their antiviral effector functions. Curr. Opin. Virol. *1*, 519–525.

Sharma, S., TenOever, B.R., Grandvaux, N., Zhou, G.P., Lin, R., and Hiscott, J. (2003). Triggering the interferon antiviral response through an IKK-related pathway. Science *300*, 1148–1151.

Shen, Y.Y., Liang, L., Zhu, Z.H., Zhou, W.P., Irwin, D.M., and Zhang, Y.P. (2010). Adaptive evolution of energy metabolism genes and the origin of flight in bats. Proc. Natl. Acad. Sci. USA *107*, 8666–8671.

Shimamoto, Y., Kitamura, H., Niimi, K., Yoshikawa, Y., Hoshi, F., Ishizuka, M., and Takahashi, E. (2013). Selection of suitable reference genes for mRNA quantification studies using common marmoset tissues. Mol. Biol. Rep. *40*, 6747–6755.

Shultz, D.B., Rani, M.R., Fuller, J.D., Ransohoff, R.M., and Stark, G.R. (2009). Roles of IKK-β, IRF1, and p65 in the activation of chemokine genes by interferon-γ. J. Interferon Cytokine Res. *29*, 817–824.

Silva-Barrios, S., Smans, M., Duerr, C.U., Qureshi, S.T., Fritz, J.H., Descoteaux, A., and Stäger, S. (2016). Innate Immune B Cell Activation by Leishmania donovani Exacerbates Disease and Mediates Hypergammaglobulinemia. Cell Rep. *15*, 2427–2437.

Simpson, D.I., and O'Sullivan, J.P. (1968). Studies on arboviruses and bats (Chiroptera) in East Africa. I. Experimental infection of bats and virus transssion attempts in Aedes (Stegomyia) aegypti (Linnaeus). Ann. Trop. Med. Parasitol. *62*, 422–431.

Stockmaier, S., Dechmann, D.K.N., Page, R.A., and O'Mara, M.T. (2015). No fever and leucocytosis in response to a lipopolysaccharide challenge in an insectivorous bat. Biol. Lett. *11*, 20150576.

Su, S., Law, C.W., Ah-Cann, C., Asselin-Labat, M.-L., Blewitt, M.E., and Ritchie, M.E. (2017). Glimma: interactive graphics for gene expression analysis. Bioinformatics *33*, 2050–2052.

Suarez, R.K., and Welch, K.C. (2017). Sugar Metabolism in Hummingbirds and Nectar Bats. Nutrients *9*, 743.

Suarez, R.K., Welch, K.C., Jr., Hanna, S.K., and Herrera M, L.G. (2009a). Flight muscle enzymes and metabolic flux rates during hovering flight of the nectar bat, Glossophaga soricina: further evidence of convergence with hummingbirds. Comp. Biochem. Physiol. A Mol. Integr. Physiol. *153*, 136–140.

Suarez, R.K., Welch, K.C., Jr., Hanna, S.K., and Herrera M, L.G. (2009b). Flight muscle enzymes and metabolic flux rates during hovering flight of the nectar bat, Glossophaga soricina: further evidence of convergence with hummingbirds. Comp. Biochem. Physiol. A Mol. Integr. Physiol. *153*, 136–140.

Sung, P.S., Cheon, H., Cho, C.H., Hong, S.-H., Park, D.Y., Seo, H.-I., Park, S.-H., Yoon, S.K., Stark, G.R., and Shin, E.-C. (2015). Roles of unphosphorylated ISGF3 in HCV infection and interferon responsiveness. Proc. Natl. Acad. Sci. USA *112*, 10443–10448.

Suu-Ire, R.D., Fooks, A.R., Banyard, A.C., Selden, D., Amponsah-Mensah, K., Riesle, S., Ziekah, M.Y., Ntiamoa-Baidu, Y., Wood, J.L.N., and Cunningham, A.A. (2017). Lagos Bat Virus Infection Dynamics in Free-Ranging Straw-Colored Fruit Bats (Eidolon helvum). Trop. Med. Infect. Dis. *2*, 25.

Swanepoel, R., Smit, S.B., Rollin, P.E., Formenty, P., Leman, P.A., Kemp, A., Burt, F.J., Grobbelaar, A.A., Croft, J., Bausch, D.G., et al. (2007). Studies of reservoir hosts for Marburg virus. Emerg. Infect. Dis. *13*, 1847–1851.

Tan, Y.F., Teng, C.L., Chua, K.B., and Voon, K. (2017). Pteropine orthoreovirus: An important emerging virus causing infectious disease in the tropics? J. Infect. Dev. Ctries. *11*, 215–219.

Tanaka, T., Murakami, K., Bando, Y., and Yoshida, S. (2015). Interferon regulatory factor 7 participates in the M1-like microglial polarization switch. Glia *63*, 595–610.

Thomas, S.P. (1975). Metabolism during flight in two species of bats, Phyllostomus hastatus and Pteropus gouldii. J. Exp. Biol. *63*, 273–293.

Voon, K., Tan, Y.F., Leong, P.P., Teng, C.L., Gunnasekaran, R., Ujang, K., Chua, K.B., and Wang, L.-F. (2015). *Pteropine orthoreovirus* infection among out-patients with acute upper respiratory tract infection in Malaysia. J. Med. Virol. *87*, 2149–2153.

Wang, P., Xu, J., Wang, Y., and Cao, X. (2017). An interferon-independent lncRNA promotes viral replication by modulating cellular metabolism. Science *358*, 1051–1055.

Weiss, G., Maaetoft-Udsen, K., Stifter, S.A., Hertzog, P., Goriely, S., Thomsen, A.R., Paludan, S.R., and Frøkiær, H. (2012). MyD88 drives the IFN-β response to Lactobacillus acidophilus in dendritic cells through a mechanism involving IRF1, IRF3, and IRF7. J. Immunol. *189*, 2860–2868.

Wu, X., Dao Thi, V.L., Huang, Y., Billerbeck, E., Saha, D., Hoffmann, H.-H., Wang, Y., Silva, L.A.V., Sarbanes, S., Sun, T., et al. (2018). Intrinsic Immunity Shapes Viral Resistance of Stem Cells. Cell *172*, 423–438.e25.

Xie, Y., He, S., and Wang, J. (2018). MicroRNA-373 facilitates HSV-1 replication through suppression of type I IFN response by targeting IRF1. Biomed. Pharmacother. *97*, 1409–1416.

Yong, K.S.M., Ng, J.H.J., Her, Z., Hey, Y.Y., Tan, S.Y., Tan, W.W.S., Irac, S.E., Liu, M., Chan, X.Y., Gunawan, M., et al. (2018). Bat-mouse bone marrow chimera: a novel animal model for dissecting the uniqueness of the bat immune system. Sci. Rep. *8*, 4726.

Yu, G., Lin, Y., Tang, Y., and Diao, Y. (2018). Comparative Transcriptomic Analysis of Immune-Related Gene Expression in Duck Embryo Fibroblasts Following Duck Tembusu Virus Infection. Int. J. Mol. Sci. *19*, 2328.

Zhang, G., Cowled, C., Shi, Z., Huang, Z., Bishop-Lilly, K.A., Fang, X., Wynne, J.W., Xiong, Z., Baker, M.L., Zhao, W., et al. (2013). Comparative analysis of bat genomes provides insight into the evolution of flight and immunity. Science *339*, 456–460.

Zhang, Q., Zeng, L.-P.P., Zhou, P., Irving, A.T.T., Li, S., Shi, Z.-L.L., and Wang, L.-F.F. (2017). IFNAR2-dependent gene expression profile induced by IFN-α in Pteropus alecto bat cells and impact of IFNAR2 knockout on virus infection. PLoS One *12*, e0182866.

Zhou, S., Cerny, A.M., Fitzgerald, K.A., Kurt-Jones, E.A., and Finberg, R.W. (2012). Role of interferon regulatory factor 7 in T cell responses during acute lymphocytic choriomeningitis virus infection. J. Virol. *86*, 11254–11265.

Zhou, P., Cowled, C., Mansell, A., Monaghan, P., Green, D., Wu, L., Shi, Z., Wang, L.-F.F., and Baker, M.L. (2014). IRF7 in the Australian black flying fox, Pteropus alecto: evidence for a unique expression pattern and functional conservation. PLoS One *9*, e103875.

Zhou, Q., Lavorgna, A., Bowman, M., Hiscott, J., and Harhaj, E.W. (2015). Aryl Hydrocarbon Receptor Interacting Protein Targets IRF7 to Suppress Antiviral Signaling and the Induction of Type I Interferon. J. Biol. Chem. *290*, 14729–14739.

Zhou, P., Tachedjian, M., Wynne, J.W., Boyd, V., Cui, J., Smith, I., Cowled, C., Ng, J.H.J., Mok, L., Michalski, W.P., et al. (2016). Contraction of the type I IFN locus and unusual constitutive expression of IFN-α in bats. Proc. Natl. Acad. Sci. USA *113*, 2696–2701.

STAR★METHODS

KEY RESOURCES TABLE

REAGENT or RESOURCE	SOURCE	IDENTIFIER
Antibodies		
Roche anti-GFP	Sigma Aldrich	Cat# 11814460001; RRID:AB_390913
Bacterial and Virus Strains		
HSV-1 Kos	ATCC	VR-1493
H1N1 IAV A/NWS/33	ATCC	VR-219
PRV3M p3	BK Chua, TLS	Prototype: taxonomy ID: 16867
MERS-CoV (HCoV-EMC/2012)	EMC	JX869059.2
Biological Samples		
P. alecto tissue (cDNA panel) – South East Queensland, Australia. (F, M)	QASP/UQ/ABC/BRQ	N/A
M. muscus tissue (cDNA panel) – C57Bl6/J	Jackson laboratories	000664
E. spelaea (cDNA) – Singapore (F,M)	Duke-NUS	N/A
Chemicals, Peptides, and Recombinant Proteins		
Pierce Protein A/G Magnetic Agarose Beads	Thermo scientific	78609
polyIC HMW	InVivoGen	tlrl-pic
IFNα3 (P. alecto) – bacterial recombinant.	CSIRO/AAHL	N/A
Lipofectamine 3000	Thermo Scientific	L3000015
IFNα3 (P. alecto) – mammalian-expressed, supernatant.	Duke-NUS	N/A
Deposited Data		
PakiT03 infection NGS (Gene Expression Omnibus)	Duke-NUS	GEO: GSE129390
P. alecto NGS (Gene Expression Omnibus)	Duke-NUS	GEO: GSE129377
E. spleaea NGS (Gene Expression Omnibus)	Duke-NUS	GEO: GSE129199
Mass spectrometry data repository	https://repository.jpostdb.org/	JPST000983
Experimental Models: Cell Lines		
PakiT03 (F) Kidney epithelial	CSIRO/AAHL	RRID: CVCL_DR89
PakiT03-variants	Duke-NUS	'Taxonomy ID: 9402
Hek293T kidney epithelial	ATCC	RRID: CVCL_0063
MdKi kidney epithelial	WIV, CAS, China	Taxonomy ID: 225400
Vero E6	Duke University	N/A
Vero B4	CCLV	RRID: CVCL_1912
Experimental Models: Organisms/Strains		
Pteropus alecto gouldii	South-East Queensland bat carers	N/A
Eonycteris spelaea	Singapore	N/A
Homo Sapiens	Published data – SRA	N/A
Oligonucleotides		
See Table S6		N/A
Recombinant DNA		
pcDNA6.2/N-EmGFP-GW/TOPO	Invitrogen	K36020
IRF1	P.a. cDNA	GenBank: XM_006923152.3
IRF3	P.a. cDNA	GenBank: XM_025048312.1
IRF7	P.a. cDNA	GenBank: NM_001320278.1
IRF5	P.a. cDNA	GenBank: XM_006910531.3

Continued

REAGENT or RESOURCE	SOURCE	IDENTIFIER
Software and Algorithms		
Bowtie2/RSEM	GitHub	v2.3.4.2
Cufflinks	GitHub	v2.2.1
HTseq-count	GitHub	0.6.1p1
Tophat	GitHub	2.1.1
EdgeR	BioConductor	3.24.3
Glimma	BioConductor	1.2.1
Prism	Graphpad	8
Biovenn	http://www.biovenn.nl/	N/A
Morpheus	https://clue.io:443/Broad	N/A
Ingenuity Pathway Analysis	QIAGEN	Summer/Fall 2019
BioDBnet	https://biodbnet-abcc.ncifcrf.gov/db/db2db.php	db2 db
GSEA	https://www.gsea-msigdb.org/gsea/msigdb/index.jsp	N/A
Other		
IFNAR2-4A: 35bp, homozygous. ATGTTTCAGATGAGCCTTGCATTTTCGAG ATAACGTTAAGAAATTTCCGGACAATTTTA TCGTGGAAATTAAAAGAC CACTCCATTGTACCAACTCACTATACATTA CAGTATGCAATCATGAG	In-House CRISPR KO – Duke-NUS	PakiT03- IFNAR2-4A
IFNAR2-9E: −70bp, homozygous TTTACCATTTCTTTTCCTTTCAAAGTGGACC AGAAGATGTCATTACTGT GAAGGACTGTACCAATATCACAAGGTCATTC TGTGACCTGACAGATG CGTGGGTGAACATGTCTGAGACGTACACTCC CAGAGTAGTCGGAC ACCGAGGGAACAGGACGCTGGTCGACTGTG AGGGCAGCTTATTCC CGTTAATGGATAGTGAGTTGACCTCTCTTTAT CATCTTCGCCATTGTC ATCAAGATCATCATTATTTTCTCTGCCATGA AATAGGCAGGTCTACACAGG	In-House CRISPR KO – Duke-NUS	PakiT03- IFNAR2-9E
IRF1-g3-2H: −44bp, homozygous. GGGGGCCAACTGGGGCTGGCATGCCCGTG CCAAGGCTAATGTCC TATCTTCCCCCCAGAGAGAAAGTCCAAGTCC AGCCGAGACGCTAAG AACAAGGCCAAGAGGAAGGTGAGTCTGGTC CTGAGCAGCTGGCCTT TGATCACCTGTGAGTCAGGGTGGGCAGTG GAAGAAGCGCC ACAGCAGCCTGGCCTAAGCTTCTTTCTCCT TCTGCA	In-House CRISPR KO – Duke-NUS	PakiT03- IRF1-g3-2H

(Continued on next page)

Continued

REAGENT or RESOURCE	SOURCE	IDENTIFIER
IRF1-g3-1A: −23bp, 21 in exons4, homozygous. GGGGGGCCAACTGGGGCTGGCATGCCCGTGC CAAGGCTAATGTC CTATCTTCCCCCCAGAGAGAAAGTCCAAGTCC AGCCGAGA CGCTAAGAACAAGGCCAAGAGGAAGGTGAGT CTGGTCCTG AGCAGCTGGCCTTGGATCACCTGTGAGTCAGG GTGGGCAG TGGAAGAAGCGCCACAGCAGCCTGGCCTAAGCT TCTTTCTCCTTCTGCA	In-House CRISPR KO – Duke-NUS	PakiT03- IRF1-g3-1A
IRF1-g3-4C: Large deletion, homozygous. 0 trace	In-House CRISPR KO – Duke-NUS	PakiT03- IRF1-g3-4C
IRF1-g4-1D: 13bp, homozygous. CCAAGAG GAAGGTGAGTCTGGTCCTGAGCAGCTGGCC TTGGATCACCTGTGAGTCAGGGTGGGCAGTGG AAGAAGCGCCACAGCAGCCTGGCCTAAGCTTC TTTCTCCTTCTGCAGTCATGTGGGGACTCCAGC CCCGATACCTTCTCCGATGGCCTCAGCAGCT CCACCCTGCCTGATGACCACAGCAGCTACACAG CTCAGGGCT ACATGGGGCAGGACTTGGAAGTTGAGAGGGCCCTT ACTCCAGGTGAGGCAGGCTGGGCC	In-House CRISPR KO – Duke-NUS	PakiT03- IRF1-g4-1D
IRF3-11C: +214, insert in exons 5, yellow region is inserted sequence. Homozygous. TGCCAAAGGGTAATGTCCTATCTTCCCCCCAGAGAGAAAG TCCAAGTCCAGCCGAGACGCTAAGAACAAGGCCAAGAGGAA GGTGAGTCTGGTCCTGAGCAGCTGGCCTTTGATCACCTGTG AGTCAGGGTGGGCAGTGGAAGAAGCGCCACAGCAGCCTG GCCTAAGCTTCTTTCTCCTTCTGCAGTCATGTGGGGACTCCA GCC CCGACCGAGGGGCCGTGTCCTCCCAGCCACACGGCAGACT GCGCCCACGTCCCGCTGCCCCCTCGCCAAGGCTGTGAGAT GCTGCCCCACGGTGGGGACACGGGACACGCCGTGAGCC CACATTCGAAAGGTCTGTGCGTTTCTCCTGCCCGGCTGGGC CAGGACTGTGACTTTGAGAAGACGTACGTCGTGAGCAGGGA CGCTGTGCGCAGGTGCCGGCCCTTCTCCGATGGCCTCAGCAG CTCCACCCTGCCTGATGACCACAGCAGCTACACAGCTCAGGG CTACATGGGGCAGGACTTGGAAGTTGAGAGGGCCCTTACTCCA GGTGAGGCAGGCTGGCCTGTAAGANCNCNNNNNNNNNNN	In-House CRISPR KO – Duke-NUS	PakiT03- IRF3-11C
IRF3-2F: −9bp, homozygous. CGCAGGTTGGACCATGGCTACCCCAAAGCCGAGGATCCTG CCCTGGCTAGTGTCGCAGCTGGACAGTGGGCAGCTGGAGGGC GTGGCATGGCTGAACGAGAGCCGCACGCGCTTTCGCATCCCT TGGAAGCACGGCTTGCGGCAGGATGCCCAGCAGGAGGACTT CGGCATCTTCCAGGTGCGCAGGAGCCAAGACTGGGCAAAC ACGGGGCGGGGCGGACTCCGAGGGCACTG	In-House CRISPR KO – Duke-NUS	PakiT03- IRF3-2F
IRF3-4B: +1, homozygous. CGCAGGTTGGACCATGGCTACCCCAAAGCCGAGGATC CTGCCCTGGCTAGTGTCGCAGCTGGACAGTGGGCAGCTG GAGGGCGTGGCATGGCTGAACGAGAGCCGCACGCGCTTTCG CATCCCTTGGAAGCACGGCTTGCcGGCAGGATGCCCAGCAGG AGGACTTCGGCATCTTCCAGGTGCGCAGGAGCCAAGAC TGGGCAAACACGGGGCGGGGCGGACTCCGAGGGCACTG	In-House CRISPR KO – Duke-NUS	PakiT03- IRF3-4B

Continued

REAGENT or RESOURCE	SOURCE	IDENTIFIER
IRF3-4G: −23bp, homozygous. CGCAGGTTGGACCATGGCTACCCCAAAGCCGAGGATCCT GCCCTGGCTAGTGTCGCAGCTGGACAGTGGGCAGCTGGA GGGCGTGGCATGGCTGAACGAGAGCCGCACGCGCTTTCG CATCCCTTGGAAGCACGGCTTGCGGCAGGATGCCCAGCAGG AGGACTTCGGCATCTTCCAGGTGCGCAGGAGCCAAGA CTGGGCAAACACGGGGCGGGGCGGACTCCGAGGGCACTG	In-House CRISPR KO – Duke-NUS	PakiT03- IRF3-4G
IRF7-3C: −17bp, homozygous. CGCCAAT CCGCGAA AGTGCACTCCGAGCCGGCTGGAAAA CCAACTTCCGCTGCGCACTGCGCAGC ACTCAGCGCTTCGTCATG CTGCACGACAATTCCGCGGACCCCGCC GACCCGCATAAAGTGT ATGAGCTCAGCTCCGAACCGCCGTGGAGAGGTAA ACAACGGGGA GGCAGCGGTCAGGGAGGGGTCAGGGAGGG GTCAGGGAGGCCA GGACGGCCAGGGCAGAGGAATGGCCTGCAC ATGCTGCTGGCACTTTGGTGGCAGCCGCTGGGTCAG	In-House CRISPR KO – Duke-NUS	PakiT03- IRF7-3C
IRF7-2G: −15bp, homozygous. CGCCAATCCGCGAAAGTGCACTCCGAGCCGGCTGG AAAACCAAC TTCCGCTGCGCACTGCGCAGCACTCAGCGCTTCGTC ATGCTGCAC GACAATTCCGCGGACCCCGCCGACCCGCATAAAGT GTATGAGCTC AGCTCCGAACCGCCGTGGAGAGGTAAACAACGGGG AGGCAGCGG TCAGGGAGGGGTCAGGGAGGGGTCAGGGAGGCCAG GACGGCCA GGGCAGAGGAATGGCCTGCACATGCTGCTGGCACTTT GGTGGCAGCCGCTGGGTCAG	In-House CRISPR KO – Duke-NUS	PakiT03- IRF7-2G
IRF7-5G: compound heterozygous, −37bp, −15bp. CGCCAATCCGCGAAAGTGCACTCCGAGCCGGCTGGAAAACCA ACTTCCGCTGCGCACTGCGCAGCACTCAGCGCTTCGT CATGCTGCA CGACAATTCCGCGGACCCCGCCGACCCGCATAAAGTG TATGAGC TCAGCTCCGAACCGCCGTGGAGAGGTAAACAACGGGG AGGCAG CGGTCAGGGAGGGGTCAGGGAGGGGTCAGGGAGGCC AGGACGG CCAGGGCAGAGGAATGGCCTGCACATGCTGCTGGCACT TTGGTGGCAGCCGCTGGGTCAG CGCCAATCCGCGAAAGTGCACTCCGAGCCGGCTGGAAAACCA ACTTCCGCTGCGCACTGCGCAGCACTCAGCGCTTCGTCATGCT GCACGACAATTCCGCGGACCCCGCCGACCCGCATAAAGTGTA TGAGCTCAGCTCCGAACCGCCGTGGAGAGGTAAACAACGGGG AGGCAGCGGTCAGGGAGGGGTCAGGGAGGGGTCAGGGAGGC CAGGACGGCCAGGGCAGAGGAATGGCCTGCACATGCTGCTG GCACTTTGGTGGCAGCCGCTGGGTCAG	In-House CRISPR KO – Duke-NUS	PakiT03- IRF7-5G

Continued

REAGENT or RESOURCE	SOURCE	IDENTIFIER
IRF7-6E: +407,homozygous. TGAGGCATTTTTCGCCAATTCCGGAAAGTGCACTTCGAG CCGGGTGGAAAACCAAATTTCGGTGCGCAATGGGCAGCACT TAGCGGTTTGTCATGGTGCACGACAATTTCGGGGACCCCGCC GAAGCCGATTCCGGCATCGCTTTCAGTGGTGGAGGATTTTGC GTGTGGCACTCCGGACAGGGACAGGCGCAGGTCACCCCGCT CCCCGTCAGCAGGTTTTTCCACTTTTTTGCTTTTCCCTTTGGGT GCCTGCCATTTGGCACTTTCCCTGGTAATTAGCACCTTGACC CCAAAGCAGCAAGGGAATCCAAAAGGGTGAGCCTCGGTTA GCAGCCGAATTGTGTGGTTTAAGAGCTTTGGGGGAAAGATT TAAAGAAAAAAAAAAAAAGTTTGGAAAAGGAAGAGGTGT CACATCCTAAGCAGTGATATGAGTATTTTAAATTTTATTTGTA GTTCAGTTGTCTGTTACCCTGACCTGCCATTAATAGGTAATTG ACAACGCATCATTATGTTTAAGGAGTTTTCTGAACCCGCATA AAGTGTATGAGCTCAGCTCCGAACCGCCGTGGAGAGGTAA ACAACGGGGAGGCAGCGGTCAGGGAGGGGTCAGGGAGGG GTCAGGGAGGCCAGGACGGCCA GGGCAGAGGAATGGCCTGCACATGCTGCTGGCACTTTGGTG GCAGCCGCTGGGTCAGGGATGTGTTGAGAAACTGTCGAAC GCCGC	In-House CRISPR KO – Duke-NUS	PakiT03- IRF7-6E
IRF7-7C: −17bp, homozygous. CGCCAATCCGCGAAAGTGCACTCCGAGCCGGCTGGA AAACCAACTTCCGCTGCGCACTGCGCAGCACTCAGCG CTTCGTCATGCTGCACGACAATTCCGCGGACCCCGCCG ACCCGCATAAAGTGTATGAGCTCAGCTCCGAACCGCCGT GGAGAGGTAAACAACGGGGAGGCAGCGGTCAGGGAG GGGTCAGGGAGGGGTCAGGGAGGCCAGGACGGCCAGG GCAGAGGAATGGCCTGCACATGCTGCTGGCACTTTGGTGG CAGCCGCTGGGTCAG	In-House CRISPR KO – Duke-NUS	PakiT03- IRF7-7C
IFNAR2/IRF7-3D: −38bp CGCCAATCCGCGAAAGTGCACTCCGAGCCGGCTGGAA AACCAACTTCCGCTGCGCACTGCGCAGCACTCAGCGCTTC GTCATGCTGCACGACAATTCCGCGGACCCCGCCGACCCGCA TAAAGTGTATGAGCTCAGCTCCGAACCGCCGTGGAGAGGTAA ACAACGGGGAGGCAGCGGTCAGGGAGGGGTCAGGGAGGG GTCAGGGAGGCCAGGACGGCCAGGGCAGAGGAATGGCC TGCACATGCTGCTGGCACTTTGGTGGCAGCCGCTGGGTCAG	In-House CRISPR KO – Duke-NUS	PakiT03-IFNAR2-4A/ IRF7-3D
IFNAR2/IRF7-2A: −17bp, same with 4G. CGCCAATCCGCGAAAGTGCACTCCGAGCCGGCTGGA AAACCAACTTCCGCTGCGCACTGCGCAGCACTCAGCGCTT CGTCATGCTGCACGACAATTCCGCGGACCCCGCCGACCCG CATAAAGTGTATGAGCTCAGCTCCGAACCGCCGTGGAGAG GTAAACAACGGGGAGGCAGCGGTCAGGGAGGGGTCAGGGA GGGGTCAGGGAGGCCAGGACGGCCAGGGCAGAGGAATGGC CTGCACATGCTGCTGGCACTTTGGTGGCAGCCGCTGGGTCAG	In-House CRISPR KO – Duke-NUS	PakiT03-IFNAR2-4A/ IRF7-2A
IFNAR2/IRF7-4F: −39bp. CGCCAATCCGCGAAAGTGCACTCCGAGCCGGCTGGAAAA CCAACTTCCGCTGCGCACTGCGCAGCACTCAGCGCTTCGTC ATGCTGCACGACAATTCCGCGGACCCCGCCGACCCGCATA AAGTGTATGAGCTCAGCTCCGAACCGCCGTGGAGAGGTAA ACAACGGGGAGGCAGCGGTCAGGGAGGGGTCAGGGAGGG GTCAGGGAGGCCAGGACGGCCAGGGCAGAGGAATGGC CTGCACATGCTGCTGGCACTTTGGTGGCAGCCGCTGGGTCAG	In-House CRISPR KO – Duke-NUS	PakiT03-IFNAR2-4A/ IRF7-4F

Continued

REAGENT or RESOURCE	SOURCE	IDENTIFIER
IFNAR2/IRF7-4G: −17bp. CGCCAATCCGCGAAAGTGCACTCCGAGCCGGCTGGAAAA CCAACTTCCGCTGCGCACTGCGCAGCACTCAGCGCTTCGT CATGCTGCACGACAATTCCGCGGACCCCGCCGACCCGCAT AAAGTGTATGAGCTCAGCTCCGAACCGCCGTGGAGAGGTAA ACAACGGGGAGGCAGCGGTCAGGGAGGGGTCAGGGAGGG GTCAGGGAGGCCAGGACGGCCAGGGCAGAGGAATGGCC TGCACATGCTGCTGGCACTTTGGTGGCAGCCGCTGGGTCAG	In-House CRISPR KO – Duke-NUS	PakiT03-IFNAR2-4A/ IRF7-4G
IRF1(g4-1D)-IRF7 B1. CATCAGCTTCCCTAACAACCTGGCACCAGCCTTTCCAGAC CAGTTTCTCAAACAACATCCCTGACCCAGCGGCTGCCACC AAAGTGCCAGCAGCATGTGCAGGCCATTCCTCTGCCCTGG CCGTCCTGGCCTCCCTGACCCCTCCCTGACCCCTCCCTGAC CGCTGCCTCCCCGTTGTTTACCTCTCCACGGCCGGTTCGGAG CTGAGCTCATACACTTTATGCGGGTAAGTATGTGGCGGGG GGGGGGGGGGCGGGCATTTACAGTGGGGAAAGATGAC AAATACTACCTCAGCCAGGTGATCAAGACCAACATCAAC AGGTAGAGACAATGTTGATGGTCTGTATCCTTTGATATGA TGTGATTAGAAGAGCACTTGACCTCTTCGGTCTTCCCGGC GGGGTCCGCGGAATTGTCGTGCAGCATGACGAAGCGC TGAGTGCTGCGCAGTGCGCAGCGGAAGT	In-House CRISPR KO – Duke-NUS	PakiT03-IRF1-g4-1D/IRF7-B1

RESOURCE AVAILABILITY

Lead Contact
Further information and requests for resources and reagents should be directed to and will be fulfilled by the Lead Contact, Lin-Fa Wang (linfa.wang@duke-nus.edu.sg).

Materials Availability
Plasmids generated for this study are available upon request with a simple MTA.
   Virus strains used in this study are commonly available and also either available upon request with MTA (e.g., PRV3M) or purchased from ATCC (e.g., H1N1).
   Monkey, human and bat cell lines and CrispR KO bat cell lines are available upon request with a simple MTA.
   DNA and RNA samples from bat cells and tissue are available for collaboration upon request with MTA.

Data and Code Availability
The accession number for the data reported in this paper is in the NCBI GEO database GEO: GSE129390 (PakiT03), #GSE129377 (*Pteropus alecto* tissue) & GEO: GSE129199 (*Eonycteris spelaea* tissue). Mass spectrometry data are available under the accession number JPST000983 at the JPOST repository https://repository.jpostdb.org/.

EXPERIMENTAL MODEL AND SUBJECT DETAILS

Animals, viruses and cells
E. spelaea were captured with the ethics approval of National University of Singapore Institutional Animal Care and Use Committee (IACUC Permit # B01/12), and the National Parks permits NP/RP11-011-3a and NP/RP12-004-2. All experiments were performed in accordance with relevant guidelines and regulations. Capturing and processing of black flying foxes (*P. alecto*) in Australia was approved by the Queensland Animal Science Precinct & University of Queensland Animal Ethics Committee (AEC#SVS/073/16/ USGMS). and the Australian Animal Health Laboratory (AAHL) Animal Ethics Committee (AEC#1389 and AEC#1557). Where possible, wild bats with irreparable physical damage (torn wings) already scheduled for euthanasia were utilized. Wild *P. alecto* bats were temporarily housed for attempted rehabilitation, adjusting to handling for several weeks. Wild-born, colony housed *E. spelaea* bats (several months) were adjusted to human handling and handling did not trigger any stress-markers/cortisol etc in the blood. Bats were age and sex-matched to the best of our ability (late juvenile for *E. Spelaea*, grown "young" adults for *P. Alecto*). Prior to processing, bats were transferred to a temperature-controlled facility, settled, euthanised and culled immediately by cardiac bleed to prevent any systemic effects from anesthesia. Processing of bats and the generation of PaKi cell lines was has been described previously (Crameri et al., 2009; Irving et al., 2019). PaKiT03 (CVCL_DR89) and variants, Hek293T (CVCL_0063) and MdKi (Liang

et al., 2015) cell lines were all cultured in DMEM (GIBCO) with 10% (v/v) FBS. All tissue was preserved in RNALater: MERS-CoV was propagated in Vero B4 (CVCL_1912) cells in DMEM, 2% FBS. At a virus-induced CPE of 80–90%, viruses were harvested, clarified by centrifugation, and the virus containing supernatant was stored at −80°C. PRV3M/Melaka Virus (p3) was propagated in Vero E6 cells and clarified as previous. Viral titers were calculated upon infectivity Vero B4 cells, by plaque assay. Human H1N1 IAV strain A/NWS/33 was purchased commercially (ATCC # VR-219). HSV-1 was propagated in HeLa cells. Human tissue data was publicly available (SAMEA2146236, SAMEA2153031, SAMEA2155751, SAMEA2159764, SAMEA2142363, SAMEA2144333, SAMEA2147920, SAMEA2155770, SAMEA2158569, SAMEA2145122, SAMEA2155590, SAMEA2162895).

METHOD DETAILS

RNA extraction and quantitative RT-PCR
Harvested tissues of mice or bats were homogenized using silicon-carbide sharp particles (BioSpec Products) in the FastPrep-24 5G Homogenizer (MP Biomedicals). RNA was extracted using either the RNEasy micro kit (QIAGEN) for tissue or the EZNA total RNA kit I (Omega Bio-tek, Norcross, GA, USA) for cell culture. Extracted RNA (500 ng) was subsequently used for cDNA synthesized using QuantiTect® Reverse Transcription Kit (QIAGEN, Germany). Reactions of qPCR were setup using the SensiFAST SYBR No-ROX Kit (Bioline, London, UK) and analyzed on the CFX96 Touch Real-Time PCR Detection System (Bio-Rad, CA, USA) under the following cycling condition: 95 °C for 5 min, followed by 40 cycles of 95 °C for 5 s and 58 °C for 30 s, and ending with a melt profile analysis. The fold change in mRNA expression was determined using the $2\text{-}\Delta\Delta Ct$ method relatively to the values in mock samples, after normalization to housekeeping genes (Geometric mean) GAPDH and SNRDP3. Samples were corrected for PCR efficiency by standard curves from sample serial dilution. Primer sequences are in the Key Resources Table.

RNaseq analysis
Total RNA was checked using the RNA 6000 LabChip Kit on the Agilent Bioanalyzer (Agilent Technologies, Palo Alto, CA). RNaseq libraries were prepared using Illumina Tru-Seq Stranded Total RNA with Ribo-Zero Gold kit following the manufacturer's instructions (Illumina, San Diego, California, USA). Libraries were validated with an Agilent Bioanalyzer (Agilent Technologies, Palo Alto, CA), diluted and applied to an Illumina flow cell using the Illumina cBOT system. Sequencing was performed on an Illumina HiSeq 3000 sequencer at the Duke-NUS Genome Biology Facility with the paired-end 150-bp read option.

After trimming and cleaning for quality assurance (including distribution of reads), all reads were mapped to the *P.alecto* reference genome (NCBI genome database: ASM32557v1, 1.01) with Bowtie and RSEM abundance estimation was performed (Li and Dewey, 2011). E. spelaea reads were denovo assembled with Tophat/Cufflinks (Ghosh and Chan, 2016) and the FPKM for both Bowtie/RSEM mapped datasets was calculated using Cufflinks followed by HTseq and edgeR (Anders et al., 2015; Robinson et al., 2010) being used to detect genes that were differentially expressed post-polyIC/PRV3M/IFN-α3 treatment, followed by visualization with the Glimma package (Law et al., 2016; Su et al., 2017). The cut-off for differentially expressed genes (DEGs) was set at > 2-fold change and p value $\leq$ 0.05. Significantly up/downregulated genes were calculated based upon Fishers t test for variance of the sample compared to Geometric mean of the three wild-type replicates compared to an array based upon the geometric mean of all genes. Basal cell lines had 3 biological replicates per cell, each treatment time point was pooled RNA from 2 biological replicates (one sample per time point). As such the DEGs were calculated for genes enriched in at least 2 time points out of 3 for IFN treatment or both time points for polyIC and PRV3M infection.

Viral plaque/titration assays
Were performed as previously described (Irving et al., 2012) using a 2 h infection followed by rinsing and then adding a 2% Methyl-cellulose (Sigma) overlay on PakiT03/Vero E6 cells in 2% FBS/DMEM for 2-4 days in triplicate in a 24-well plate with a 10-fold dilution series. 0.8% Carboxy-methyl-cellulose was used for PRV3M (Melaka virus, parental strain) with Vero B4 cells. PRV3M and MERS-CoV (EMC/2012) titers were determined by limiting dilution. In brief, tenfold serial diluted virus was added into a 96-well plate containing 1×10^4 Vero B4 cells per well. Cells were observed for cytopathatic effect and the titers were expressed as $TCID_{50}$ ml^{-1}. All work with live MERS-CoV was performed in BSL3 containment at SingHealth Experimental Medical Centre.

Viral infection/ligand stimulation assays
PolyIC stimulation (1mg/ml), IFNα3 treatment and infection with HSV/IAV were done as previously (Zhang et al., 2017). PRV3M/MERS-CoV infection was performed using the same method with an MOI of 0.1 or 1 (as detailed) for various time points. Supernatant was collected for titration as mentioned previously. Cells were lysed directly in TRK RNA lysis buffer.

Mass spectrometry analysis
WT and KO cells were treated with polyIC or *P. alecto* IFNα3, as previous, overnight (16h). Cells were lysed in Buffer (Irving et al., 2012) followed by precipitation and concentration and bound proteins were denatured directly in 8 M urea/50 mM Tris-HCl buffer pH 8.0. Proteins were reduced with 25 mM TCEP for 20 min at 25°C and alkylated with 55 mM 2-chloroacetamide (CAA) for 30 min, in the dark, at room temperature. Before digestion, samples were diluted with 100 mM triethylamonium bicarbonate buffer (TEAB). Protease digestion was carried out with LysC enzyme (Wako) for 4 h, followed by trypsin (Promega) treatment for 18 h at 25°C (1:100, en-

zyme:protein ratio). Subsequently, samples were acidified with 1% trifluoroacetic acid and peptides were desalted by Sep-Pak C18 cartridges (Waters). Elution of peptides was performed with 0.5% acetic acid, 80% acetonitrile followed by peptide concentration using a vacuum concentrator system (Eppendorf). For quantitative mass spectrometry samples were labelled with TMT isobaric mass tag reagent (Thermo). Labelling was performed according to the manufacturer instruction. Following labelling, combined peptides were fractionated using in-house prepared high pH reverse phase columns (Reposil-Pur Basic C18 10μm, Dr Maisch Gmbh). Samples were eluted in 11 fractions of increasing concentration of acetonitrile (7%, 10%, 12%, 15%, 17%, 20%, 22%, 25%, 27%, 30%, 50%) in 10mM ammonium formate. Peptides were washed with 70% acetonitrile in 0.1% Formic Acid twice. Vacuum dried peptides were subsequently analyzed on an EASY-n LC 1000 (Thermo) chromatography system coupled with Orbitrap Fusion mass spectrometer (Thermo). Each fraction was separated in 120 min gradient (0.1% formic acid in water and 99.9% acetonitrile with 0.1% formic acid) using a 50 cm × 75 μm inner diameter EASY-Spray Reverse Phase Column (C-18, 2 μm particles, Thermo). For acquisition, an Orbitrap analyser with ion targets and resolution (OT-MS 4e5 ions 60k; OT-MS/MS 5e5 ions 50k) was used. Data was acquired in speed mode: cycle time 3 sec.

MS-data analysis
Thermo Proteome Discoverer software (v 2.2, Thermo Fisher Scientific) was used to generate peak lists followed by combined search using Mascot 2.6.1 engine (Matrix Science) against target-decoy Bat customized database with following parameters: Fixed modifications: Carbamidomethyl cysteine and TMT10-plex labelling on N-terminus peptide and Lysine. Variable modifications: Oxidated (M), Deamidated (NQ) and acetylated protein N-terminus were set as variable modifications. Mass accuracy for MS 20ppm, for fragment ions MS/MS 0.06Da, Enzyme: Trypsin/P with 3 missed cleavages allowed. FDR cut off for PSM and peptides was of 1% for high and 5% for medium confidence peptides.

CRISPR Knockout cell line generation
Guide RNA design, vector construction, transfection, single cell screening and validation were done as described previously (Zhang et al., 2017). Validated clones & sequences are in the Key Resources Table.

IRF overexpression and luciferase studies
IRF-GFP fusions constructs were generated in pCDNA6.2/emGFP-GW/D-Topo (Invitrogen) as described previously (Zhou et al., 2014), except for IRF1/5 that were cloned using the same methodology from PakiT03 cDNA (#XM_006923152.3, XM_006910531.3 respectively). Luciferase assays were as described previously in Hek293T cells (low baseline IRF expression). Cells were adhered to pre-cleaned glass confocal coverslips #1.5 in the bottom of 24-well plates or imaged directly on plastic tissue culture 24-well plates (for low magnification). Cells were treated as previously, rinsed with pre-warmed PBS (37°C), and fixed with 4% Paraformaldehyde 0.37% Gluteraldehyde (pre-warmed) for 20 minutes). Cells in plates were imaged directly in PBS, coverslips were mounted using Mowiol-4.88.

Pathway analysis
Pathway analysis was performed with EnrichR (https://maayanlab.cloud/Enrichr/) using significant DEGs as a list and the clustergram for CHEA and ENCODE consensus was used for TF/gene correlations. GSEA signatures were downloaded from m = MSigDB Hallmark/curated sets and gene lists were aligned, recording the k/K values and the FDR Q-value. Ingenuity Pathway Analysis was used by projecting bat gene ID onto human HGNC symbols (biodbnet) and average fold induction of genes (relative to untreated) was used in conjunction with P value or relative to WT cells (for proteomics). Only direct relationships were considered and highly significant/inferred data, excluding possible mutation analysis. Upstream regulator analysis included both genes and endogenous chemicals. Both Z-score for expression-weighted analysis and pure significance (P value) was collected and represented as indicated in the figure legends (complete values in supplemental tables).

QUANTIFICATION AND STATISTICAL ANALYSIS

Unless specifically mentioned in the figure legend all experiments were performed in a biological (n) triplicate with multiple replicates ≥ 3. Graphs for qPCR are combined for technical duplicates x 3-4 replicates, normalized across housekeeping geometric mean. Graphs were generated using Graphpad Prism and unless otherwise stated statistics is calculated using unpaired, two-tailed t test's without correction for variance. Error is represented as SEM unless otherwise stated and p* < 0.05, ** < 0.02, *** < 0.01. Heatmaps were generated in Morpheus (https://clue.io:443/ Broad Institute) and the scale is based upon Min/Med/Max, unless otherwise indicated, and displayed in each figure. Normalized heatmaps across species were calculated as fold expression relative to housekeeping for a Geometric mean of 13 housekeeping genes considered appropriate for cross-species/tissue comparison (Caracausi et al., 2017; Eisenberg and Levanon, 2013; Shimamoto et al., 2013), values are in the Supplemental tables. Venn Diagrams were generated by Glimma or BioVenn for weighted VennDiagrams.